CELL BIOLOGY

RAB7A phosphorylation by TBK1 promotes mitophagy via the PINK-PARKIN pathway

J.-M. Heo[1], A. Ordureau[1], S. Swarup[1], J. A. Paulo[1], K. Shen[2,3,4,5], D. M. Sabatini[2,3,4,5], J. W. Harper[1]*

Removal of damaged mitochondria is orchestrated by a pathway involving the PINK1 kinase and the PARKIN ubiquitin ligase. Ubiquitin chains assembled by PARKIN on the mitochondrial outer membrane recruit autophagy cargo receptors in complexes with TBK1 protein kinase. While TBK1 is known to phosphorylate cargo receptors to promote ubiquitin binding, it is unknown whether TBK1 phosphorylates other proteins to promote mitophagy. Using global quantitative proteomics, we identified S72 in RAB7A, a RAB previously linked with mitophagy, as a dynamic target of TBK1 upon mitochondrial depolarization. TBK1 directly phosphorylates RAB7A^{S72}, but not several other RABs known to be phosphorylated on the homologous residue by LRRK2, in vitro, and this modification requires PARKIN activity in vivo. Interaction proteomics using nonphosphorylatable and phosphomimetic RAB7A mutants revealed loss of association of RAB7A^{S72E} with RAB GDP dissociation inhibitor and increased association with the DENN domain–containing heterodimer FLCN-FNIP1. FLCN-FNIP1 is recruited to damaged mitochondria, and this process is inhibited in cells expressing RAB7A^{S72A}. Moreover, nonphosphorylatable RAB7A failed to support efficient mitophagy, as well as recruitment of ATG9A-positive vesicles to damaged mitochondria. These data reveal a novel function for TBK1 in mitophagy, which parallels that of LRRK2-mediated phosphorylation of the homologous site in distinct RABs to control membrane trafficking.

INTRODUCTION

Elimination of particular types of damaged mitochondria occurs through a specialized form of autophagy referred to as "mitophagy." The best understood form of mitophagy is orchestrated by the PINK1 protein kinase and the PARKIN ubiquitin (Ub) ligase, two genes that are mutated in early-onset Parkinson's disease (*1*, *2*). In healthy mitochondria, PINK1 is imported through the mitochondrial protein import translocon and rapidly degraded (*3*). Upon mitochondrial damage such as depolarization, PINK1 is stabilized on the mitochondrial outer membrane (MOM) and can catalyze the phosphorylation of S65 in both preexisting Ub and the Ub-like domain (Ubl) of PARKIN [reviewed in (*1*, *2*, *4*)]. These modifications activate PARKIN-dependent ubiquitylation of numerous MOM proteins by PARKIN through a "feed-forward" mechanism involving both recruitment of cytosolic PARKIN to the MOM via interaction with pS65-Ub and accumulation of pS65-Ub as PARKIN increases the abundance of Ub chains on the MOM (*1*, *2*, *4*).

A key rate-limiting step in mitophagy is the recruitment of Ub-binding autophagy cargo receptors—typified by OPTN, CALCOCO2 (also called NDP52), and SQSTM1 (also called p62)—to the MOM (*5*–*9*). These cargo receptors contain two important functional domains: an "LC3 interaction region" (LIR) that is capable of interacting with ATG8 proteins (LC3A, LC3B, LC3C, GABARAP, GABARAPL1, and GABARAPL2) and one of several types of Ub chain binding domains, including UBAN in OPTN and UBA in SQSTM1 (*2*, *10*, *11*). The ability of these Ub-binding receptors to promote efficient mitophagy requires the TBK1 kinase, which associates with and phosphorylates the receptors upon their binding to Ub chains (*6*, *7*, *9*, *12*, *13*). In the case of OPTN, phosphorylation within the UBAN domain (S473 and S513) increases the affinity of OPTN for K63-Ub chains, which is thought to facilitate the mitophagy process by increasing the residence time of receptors on the MOM (*7*, *9*, *11*). Moreover, OPTN is dynamically phosphorylated by TBK1 on S177, adjacent to the LIR motif, leading to increased affinity for ATG8 proteins (*7*, *12*, *14*). Experiments in HeLa cells expressing PARKIN indicate that TBK1–cargo receptor complexes are recruited to a subset of fragmented mitochondria within 1 hour of depolarization, and in this context, TBK1 is phosphorylated on S172 to activate its catalytic activity (*6*, *7*). Thus, the assembly of Ub chains on the MOM by PARKIN promotes a second phosphorylation-driven feed-forward loop that supports both TBK1 activation within mitochondrial "puncta" and enhanced binding of cargo receptors such as OPTN to Ub chains (*1*, *2*, *11*). A similar mechanism involving TBK1 and OPTN has also been implicated in the detection of cytosolic bacteria to promote xenophagy (*9*, *11*, *15*) or in innate immunity (*14*). Mutations in *TBK1*, *OPTN*, and *SQSTM1* have been genetically linked with amyotrophic lateral sclerosis, and patient mutations in TBK1 and OPTN often disrupt their association, pointing to an important role for this signaling module in removal of autophagy cargo in disease (*11*).

The activation of TBK1 within OPTN/SQSTM1-positive puncta on damaged mitochondria (*7*) raised the question of whether TBK1 has substrates other than cargo receptors within the vicinity of ubiquitylated mitochondria. Here, we report the use of phosphoproteomics to search for TBK1 targets in response to mitochondrial depolarization in HeLa cells, leading to the identification of S72 in RAB7A as a dynamic physiological target of TBK1 in this context. Although best understood as a RAB involved in maturation of endosomes downstream of RAB5, multiple studies have linked RAB7A to membrane fusion events involving other classes of membranes, including mitophagy. RAB7A is recruited to damaged mitochondria in a CCZ1-MON1–dependent manner, where it interacts with and is acted upon by mitochondrial-tethered guanosine triphosphatase (GTPase) activating proteins (GAPs) TBC1D15/17,

[1]Department of Cell Biology, Harvard Medical School, Boston, MA 02115, USA. [2]Whitehead Institute for Biomedical Research and Department of Biology, Massachusetts Institute of Technology, Cambridge, MA 02142, USA. [3]Howard Hughes Medical Institute, Department of Biology, Massachusetts Institute of Technology, Cambridge, MA 02139, USA. [4]Koch Institute for Integrative Cancer Research, Massachusetts Institute of Technology, Cambridge, MA 02142, USA. [5]Broad Institute of Harvard and MIT, Cambridge, MA 02142, USA.
*Corresponding author. Email: wade_harper@hms.harvard.edu

and depletion of RAB7A reduces PARKIN-dependent mitophagic flux (*16*–*18*) and is also recruited to autophagosomes via CCZ1-MON1 (*19*). RAB7A function has been linked to accumulation of ATG9A on damaged mitochondria (*17*, *18*). ATG9A is a multipass transmembrane protein that forms on vesicles emerging from the Golgi, and these vesicles are thought to serve as a source of autophagosomal membranes upon phagophore nucleation via VPS34–phosphoinositide 3-kinase complex, ULK1 protein kinase, and WD repeat domain phosphoinositide-interacting protein (WIPI) (*20*). The release of RAB7A from endosomes and its ability to mobilize ATG9A from the Golgi rely upon the retromer complex (*18*).

RAB7A^{S72} is located in the "switch II" domain, which is involved in both guanosine diphosphate (GDP)/guanosine triphosphate (GTP) exchange and interactions with other proteins. A phosphorylatable residue is found in a large fraction of RABs at the equivalent position. The LRRK2 protein kinase, also mutated in Parkinson's disease, phosphorylates the analogous position in a distinct set of RABs including RAB1A, RAB1B, and RAB8A to control their interaction with regulatory factors (*21*, *22*). We demonstrate that recombinant TBK1 phosphorylates S72 in RAB7A, but not other RABs known to be phosphorylated by LRRK2, in vitro, and is required for RAB7A phosphorylation in cells in a manner that requires assembly of Ub chains on mitochondria by PARKIN. Quantitative interaction proteomics using nonphosphorylatable and phosphomimetic RAB7A^{S72} mutants revealed loss of interaction between RAB7A^{S72E} and RAB GDP dissociation inhibitors (GDIs) and an increase in the association between RAB7A^{S72E} and the FLCN/FNIP1 complex. Both FLCN and FNIP1 are enigmatic members of a small family of proteins distantly related to DENN domain proteins that function as guanine nucleotide exchange factors (GEFs) for particular RABs. Thus far, GEF activity of FLCN has only been observed for RAB35 (*23*), and moreover, other studies suggest that FLCN-FNIP1 functions as a GAP for RAG family GTPases on the lysosome (*24*, *25*). We find that the FLCN-FNIP1 complex is also recruited to mitochondria in response to depolarization, but cells harboring nonphosphorylatable RAB7A^{S72A} mutants are unable to support depolarization-dependent recruitment of FLCN/FNIP1 to mitochondria and are defective in mitophagic flux, as are cells lacking FLCN. Moreover, RAB7A^{S72A} cells are defective in the accumulation of ATG9A on mitochondria, indicating that phosphorylation of RAB7A^{S72} is critically linked to RAB7A's primary known function in mitophagy (*16*–*18*), although FLCN-FNIP1 does not appear to be required for ATG9 recruitment. Together, these data indicate that TBK1, via phosphorylation of RAB7A^{S72}, promotes downstream steps in capture of damaged mitochondria for mitophagy and reveal parallel regulatory modifications occurring on distinct RABs through kinases implicated in multiple neurodegenerative diseases.

RESULTS

Activation of the PINK1-PARKIN system transiently activates a small pool of TBK1

Previous studies have demonstrated that TBK1 is phosphorylated on S172 in response to mitochondrial depolarization within 1 hour, and this event requires the ability of its associated OPTN to bind PARKIN-dependent Ub chains through its UBAN domain (*7*, *9*). However, the kinetics and stoichiometry of TBK1 activation have not been investigated. We initially found in HeLa Flip-In TRex (HFT) cells inducibly expressing PARKIN^{WT} that TBK1 is activated 1 hour after depolarization with antimycin A/oligomycin A (AO), as observed using immunoblotting with α-pS172 TBK1 antibodies, but TBK1^{S172} phosphorylation returned to baseline within 2 hours (Fig. 1A). Increased TBK1^{S172} phosphorylation was initially detectable at 30 min after depolarization, which correlated with the initial detection of Ub chains on PARKIN targets CISD1 and TOMM20, was maximal at 60 min, and was reduced to 50% of maximum by 90 min (Fig. 1B).

To determine the stoichiometry of TBK1 phosphorylation, we first used CRISPR-Cas9–based gene editing to create homozygous N-terminally tagged enhanced green fluorescent protein (EGFP)–TBK1 in HFT cells with or without PINK1 (Fig. 1C), thereby allowing efficient purification of EGFP-TBK1 for proteomic analysis using immobilized α-GFP antibodies. As expected, the EGFP-TBK1 protein displayed increased phosphorylation 1 hour after depolarization to an extent similar to that seen with endogenous TBK1, as observed using immunoblotting with α-pS172 TBK1 antibody, and this modification was fully dependent on PINK1 (Fig. 1D). As expected, EGFP-TBK1 was diffusely localized in the cytoplasm in untreated cells but was recruited into puncta that colocalized with mitochondria upon 1 hour of depolarization (fig. S1A), analogous to puncta observed previously with α-pS172 TBK1 antibodies (*7*). To quantify TBK1 phosphorylation, we developed heavy reference tryptic peptides that allow measurement of the total abundance of TBK1 and the abundance of the tryptic peptide containing pS172 (TBK1$^{163–187}$) using parallel reaction monitoring (PRM)–based proteomics. At 1 hour after depolarization, S172 phosphorylation increased threefold from the unstimulated level (Fig. 1E), with a stoichiometry of 0.0012 (Fig. 1F). Thus, a small cytosolic pool of TBK1 is dynamically phosphorylated upon mitochondrial depolarization in a process that requires PARKIN and PINK1 activity, as well as the ability of associated OPTN to bind Ub chains.

A phosphoproteomic screen identifies RAB7A^{S72} as a candidate TBK1 target during PINK1-PARKIN–dependent mitophagy

TBK1 has been shown to phosphorylate associated autophagy cargo receptors, including SQSTM1 and OPTN, in response to mitochondrial depolarization, and is rapidly recruited to ubiquitylated mitochondria together with cargo receptors (*7*, *9*). To search for additional proteins that could be targeted by TBK1 within the context of its activation on mitochondria, we used a quantitative proteomic approach using tandem mass tagging (TMT) (Fig. 1G) (*26*). Duplicate cultures of HFT-PARKIN^{WT} cells with or without TBK1 were either left untreated or depolarized for 1 hour, and an additional culture of each was depolarized for 90 min (Fig. 1G). Total Lys-C/tryptic peptides were enriched for phosphopeptides using immobilized TiO_2 before TMT proteomics, resulting in the quantification of 10,151 phosphopeptides from 7256 proteins (Fig. 1H and data file S1). In parallel, total proteome analysis was performed using TMT, allowing the extent of phosphorylation to be normalized against the total protein abundance under the two treatment conditions (data file S2). As expected (*27*), the pS65-Ub peptide was markedly induced at 60 and 90 min (20- and 35-fold, respectively, in a TBK1-independent manner) (Fig. 1I). We also detected about two- to threefold increases in the abundance of phosphopeptides derived from SQSTM1 at 1 hour after depolarization, containing single or dual phosphorylation of S282, S283, or S288 that was completely TBK1 dependent (Fig. 1J and fig. S1B). We detected a fivefold increase in

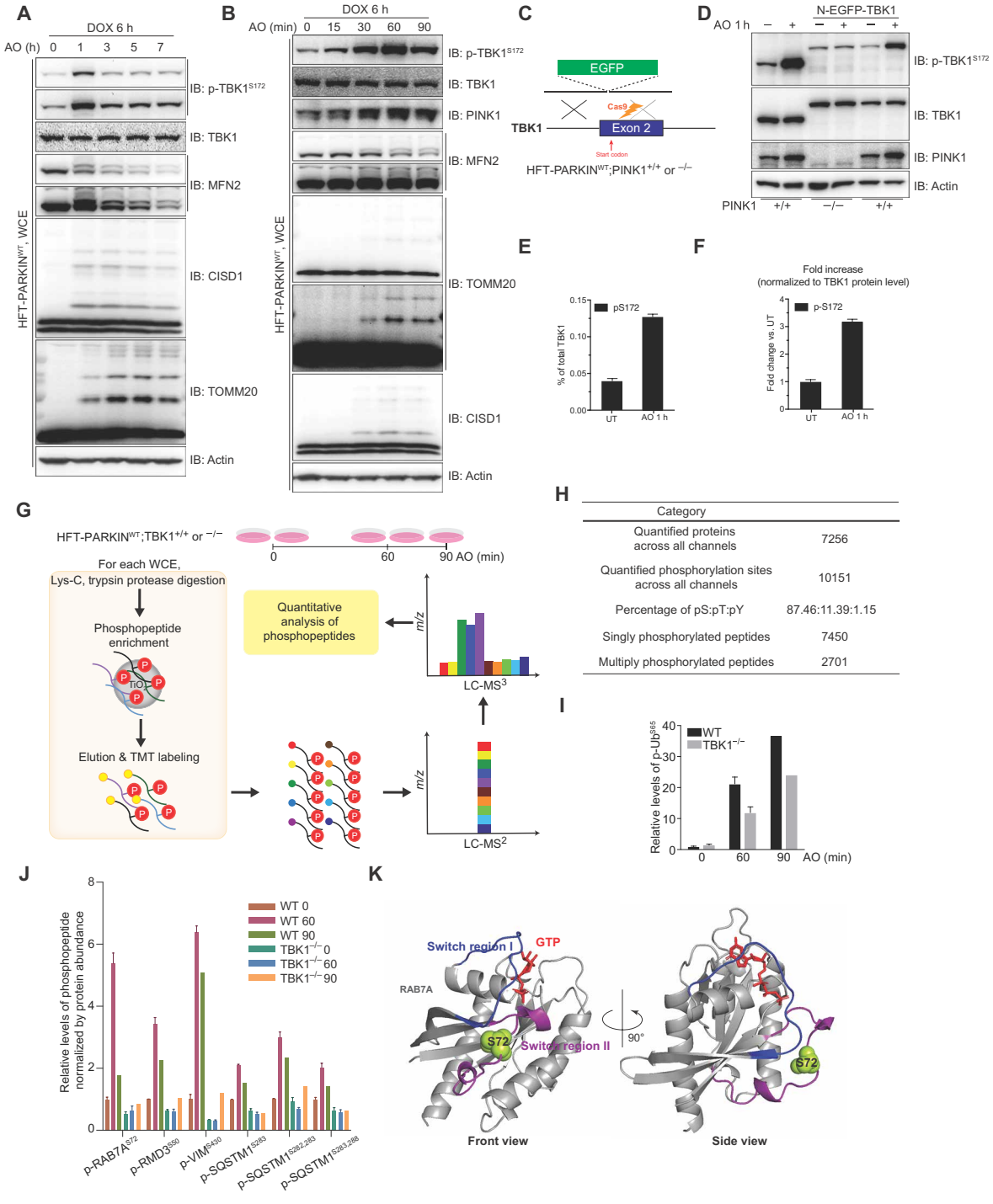

Fig. 1. TBK1 is dynamically activated in response to mitochondrial depolarization and promotes phosphorylation of RAB7A on S72 within switch II. (**A** and **B**) HFT PARKIN^{WT} cells treated with doxycycline (DOX) were depolarized with AO for the indicated periods of time before analysis of whole-cell extracts (WCE) by SDS–polyacrylamide gel electrophoresis (PAGE) using the indicated antibodies. (**C**) Schematic for the creation of HFT-PARKIN^{WT} cells (with or without previous deletion of PINK1) expressing GFP-TBK1 using CRISPR-Cas9. (**D**) HFT-PARKIN^{WT} cells with or without either PINK1 or GFP-TBK1 were depolarized with AO for 1 hour before immunoblotting (IB) of whole-cell extracts with the indicated antibodies. (**E** and **F**) Quantitative analysis of pS172 in TBK1 in the presence and absence of AO (1 hour) was performed using PRM. Error bars represent SEM from biological triplicate measurements. UT, untreated. (**G**) Schematic workflow for TBK1-dependent phosphoproteome discovery. Whole-cell extracts from the indicated cells (duplicates for untreated and 1-hour treatments and a single replicate for 1.5 hours of depolarization) were cleaved with Lys-C and trypsin, phosphopeptides were enriched using TiO_2, and samples were labeled for 10-plex TMT before analysis using SPS-MS^3 (*26*). *m/z*, mass/charge ratio. (**H**) Peptide and protein quantification from TMT proteomics of experiment outlined in (G). (**I**) Dynamics of pS65-Ub in response to mitochondrial depolarization from the experiment outlined in (G). (**J**) Dynamics of phosphorylation sites in RAB7A, RMD3, VIM, and SQSTM1 from the experiment outlined in (G). (**K**) Structure of RAB7A (Protein Data Bank: 1T91) showing the location of switch I in blue, switch II in magenta, S72 in green, and GTP in red.

the phosphorylation of S72 in RAB7A at 1 hour after depolarization after normalizing for total RAB7A protein abundance (Fig. 1J and fig. S1B). This modification had return to near baseline levels at 90 min and was completely dependent on the presence of TBK1 (Fig. 1J).

S72 in RAB7A is located in the switch II region of the protein (Fig. 1K). Switch II regions in small GTPases are known to interact with effectors when in the GTP-bound form (*28*, *29*). This position is highly conserved as a phosphorylatable S or T residue across small GTPases (fig. S1C), and the homologous residue in several other RABs has been shown to be phosphorylated by LRRK2 (*21*, *22*). In addition, previous large-scale phosphoproteomic studies identified RAB7 S72 phosphorylation in response to either interferon or Toll-like receptor activation, but the kinases involved were not identified (*30*, *31*).

A pool of RAB7A is dynamically phosphorylated in vivo in a TBK1-, PARKIN-, and PINK1-dependent manner upon mitochondrial depolarization

Given that RAB7A has been previously linked with multiple steps in autophagy and is known to be recruited to depolarized mitochondria (*16*–*18*, *32*), we sought to validate its phosphorylation by TBK1 and to explore the role of RAB7A phosphorylation in mitophagy. To facilitate this analysis, we deleted RAB7A in HFT-PARKIN^{WT} cells and reexpressed N-terminally FLAG-hemagglutinin (HA)–tagged RAB7A^{WT}, the nonphosphorylatable S72A mutant, or the potential phosphomimetic S72E using a murine stem cell virus (MSCV) retrovirus at near endogenous levels, as assessed by immunoblotting (Fig. 2, A and B). Initially, we developed a PRM assay for quantification of the extent of RAB7A phosphorylation on S72 using α-FLAG–purified FLAG-HA-RAB7A. Using this assay, we detected a 4.5-fold increase in S72 phosphorylation at 1 hour after depolarization, with a stoichiometry of 0.0056, indicating that a small pool of cytosolic RAB7A is subject to this dynamic modification (Fig. 2, C to E, and fig. S1D), consistent with immunofluorescence studies (*17*). Using Phostag-PAGE analysis of cell extracts, we observed a depolarization-dependent decrease in mobility for a small fraction of FLAG-HA-RAB7A^{WT} that was absent from cells expressing FLAG-HA-RAB7A^{S72A}, as detected using either α-HA or α-RAB7A antibodies. The appearance of this low-mobility species on Phostag-PAGE was also absent in TBK1$^{-/-}$ cells (Fig. 2F).

Given that TBK1 activation in response to mitochondrial depolarization is dependent on PINK1 and PARKIN (*7*), we performed a phosphoproteomic analysis of depolarized mitochondria using 10-plex TMT-based quantification. Duplicate cultures of HFT-PARKIN^{WT} or enzymatically defective PARKIN^{S65A} cells, or HFT-PARKIN^{WT};PINK1$^{-/-}$ cells, were left untreated or depolarized for 1 or 6 hours before purification of mitochondria and proteomic analysis (Fig. 2G and data file S3) (*33*). As shown in the −log(*P* value) versus log$_2$FC 1-hour AO/untreated plots normalized for total protein abundance performed in parallel, the peptide for pS65-Ub was markedly induced (Fig. 2H), consistent with pathway activation. The peptide for pS72 in RAB7A was also increased in depolarized PARKIN^{WT} cells but not in PINK1$^{-/-}$ or PARKIN^{S65A} cells and was also not significantly increased 6 hours after depolarization (Fig. 2, G to I, and fig. S1, D and E), consistent with its dynamic phosphorylation. Together, these data indicate that activation of TBK1 upon mitochondrial depolarization leads to phosphorylation of a small pool of RAB7A on S72, and this relies on PINK1-PARKIN activity.

TBK1 directly and specifically phosphorylates RAB7A^{S72} in vitro

We next sought to examine whether RAB7A is a direct substrate of TBK1 in vitro. Glutathione *S*-transferase (GST)–RAB7A^{WT} and the S72A mutant were purified from *Escherichia coli* (Fig. 3A), and kinase assays were performed using recombinant GST-TBK1 and TcPINK1 in parallel. GST-TBK1 addition resulted in an adenosine triphosphate (ATP)–dependent reduction in the mobility of GST-RAB7A^{WT} on Phostag-PAGE, and this was not observed with GST-RAB7A^{S72A} or when TcPINK1 was used as the kinase (Fig. 3B).

Previous studies have indicated that LRRK2 can phosphorylate the homologous residue in several RABs, including RAB1A, RAB1B, and RAB8A (*21*, *22*). All RAB substrates for LRRK2 contain a Thr at this position, and LRRK2 is inactive toward RABs with Ser at this position (*21*). We therefore examined whether TBK1 could also phosphorylate these proteins, as well as RAB7L, which is a risk factor for Parkinson's disease, on the homologous residue (Fig. 3, C to G). Surprisingly, TBK1 was specific for RAB7A with respect to phosphorylation of S72 or its equivalent, although TBK1 did create more slowly migrating forms of these proteins that were unchanged in the S72A equivalent mutants. Previously, RAB8A was shown to be phosphorylated on S111 by unknown kinase downstream of PINK1 activation (*34*). We wondered if TBK1 could be responsible for this event and performed an in vitro kinase assay using RAB8A^{WT} and nonphosphorylatable RAB8A^{S111A}. As shown in Fig. 3G, we did not detect distinct slower migrating bands appearing in RAB8A^{WT} when compared with RAB8A^{S111A} using Phostag-PAGE, suggesting that RAB8A is not a direct target of TBK1. Together, these data indicate that S72 in RAB7A is a target of TBK1 and that TBK1 displays some selectivity for phosphorylation of this site in RAB7A relative to other related RABs. Moreover, it appears that S72 is the only residue in RAB7A phosphorylated by TBK1.

Altered protein interactions for nonphosphorylatable and phosphomimetic forms of RAB7A^{S72}

Given that switch II in RABs is thought to interact with effectors and that S72A and S72E mutants in other RABs affect protein interactions (*21*, *28*), we next examined whether these forms of RAB7A display alterations in interacting partners. HFT-PARKIN^{WT};RAB7A$^{-/-}$ cells expressing FLAG-HA-RAB7A proteins at near endogenous levels (in triplicate) were left untreated or depolarized for 1 hour and individually immunoprecipitated with α-FLAG M2 magnetic beads after cell lysis with either 1% Triton X-100 or 0.5% NP-40 before TMT-based quantitative proteomics. Volcano plots for individual proteins enriched or reduced in α-FLAG immune complexes are displayed in Fig. 4 (A and B). We found broad agreement between the two detergents (Fig. 4, A and B; fig. S2, A and B; and data file S4). In both untreated and depolarized cells, we observed two major alterations in associated proteins.

First, the phosphomimetic RAB7A^{S72E}, but not RAB7A^{S72A}, displayed an increase in association with the DENN domain–containing FLCN/FNIP1 complex (Fig. 4, A to C, and data file S4). Increased association of the phosphomimetic was validated using immunoprecipitation followed by immunoblotting (Fig. 4D). We validated an increased affinity between FLCN and pS72-RAB7A using GST-pS72-RAB7A produced in *E. coli* using amber codon suppression at codon 72 with pSer-charged transfer RNAs (tRNAs) (*35*). The purified GST-pS72-RAB7A displayed a phosphorylation stoichiometry of 0.7 based on PRM, and addition of calf intestinal phosphatase led

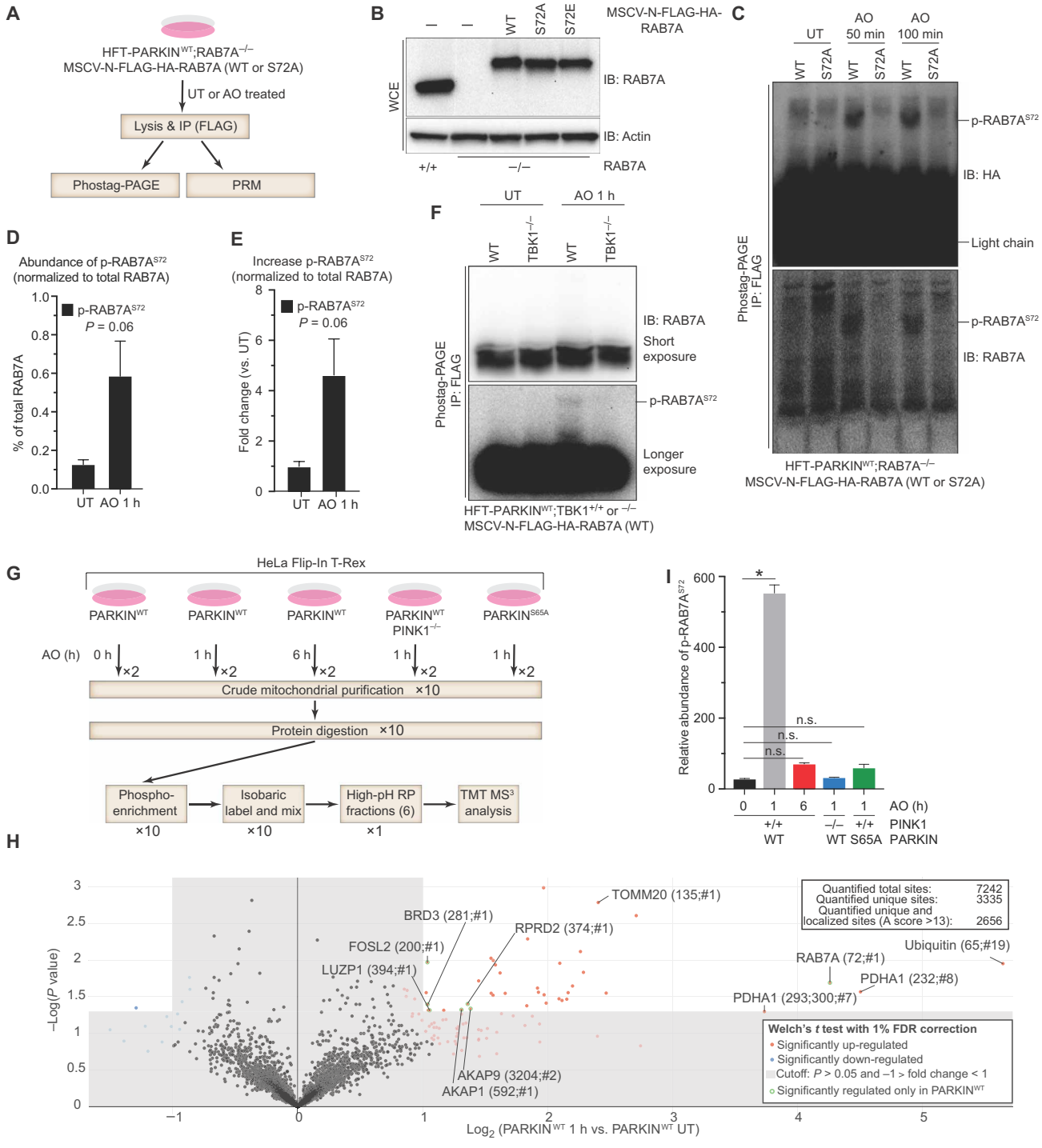

Fig. 2. Dynamic phosphorylation of a pool of RAB7A on S72 in vivo in response to mitochondrial depolarization requires PARKIN and PINK1. (**A**) Schematic for experiments examining the phosphorylation of S72 in RAB7A by TBK1. The indicated cells were subjected to depolarization, and cell extracts were subjected to α-FLAG immunoprecipitation (IP) before either Phostag-PAGE or PRM proteomics. (**B**) Immunoblotting of whole-cell extracts from the indicated cells using α-RAB7A or α-actin as a loading control. (**C**) α-FLAG immunoprecipitates from the indicated cells were separated by Phostag-PAGE followed by immunoblotting with the indicated antibodies. (**D** and **E**) Quantitative analysis of pS72 in RAB7A in the presence and absence of AO (1 hour) was performed using PRM. Error bars represent SEM from triplicate measurements. (**F**) TBK1 requirement for RAB7A^{S72} phosphorylation in response to AO (1 hour). The indicated cells were subjected to depolarization, and cell extracts were subjected to α-FLAG immunoprecipitation before Phostag-PAGE and immunoblotting with α-RAB7A antibodies. (**G**) HFT-PARKIN^{WT} or S65A cells with or without PINK1 were depolarized for the indicated times and purified mitochondria enriched for phosphopeptides using immobilized metal anion chromatography (IMAC) before TMT-based proteomics. RP, reversed-phase. (**H**) Volcano plot of −log(*P* value) versus the $\log_2$FC (fold change) for quantified phosphopeptides for PARKIN^{WT} cells with or without AO treatment for 1 hour. Phosphorylation site and number of peptides quantified are shown in parenthesis. (**I**) Relative abundance of pS72 RAB7A normalized to RAB7A abundance also measured by TMT. Error bars represent SEM from biological triplicate measurements. n.s., not significant.

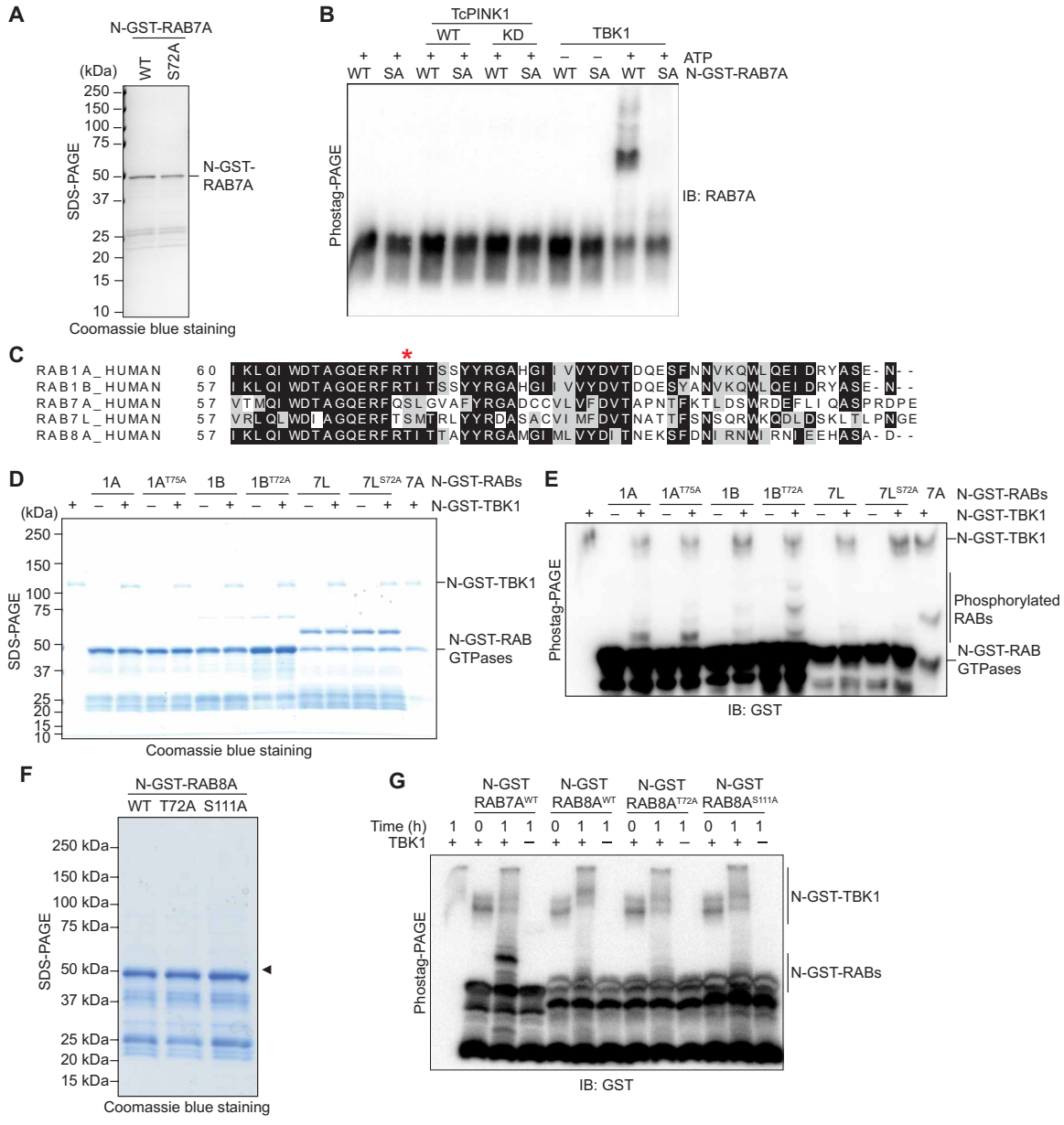

Fig. 3. TBK1 phosphorylates RAB7A^{S72} but not the equivalent residue in other RABs in vitro. (**A**) Coomassie blue PAGE analysis of purified GST-RAB7A^{WT} and RAB7A^{S72A} after purification from *E. coli*. (**B**) The indicated GST-RAB7A proteins were incubated with recombinant TcPINK1 (*E. coli*) (*27*) or GST-TBK1 (insect cells) (1 hour at 30°C, with or without ATP), and reaction products were separated by Phostag-PAGE before immunoblotting with α-RAB7A antibody. (**C**) Alignment of the amino acid sequence around S72 in RAB7A (red asterisk) and selected RABs. (**D**) Coomassie blue SDS-PAGE analysis of purified GST-RAB1A, GST-RAB1B, and GST-RAB7L (with or without mutation of the S72 equivalent to Ala) after purification from *E. coli*. (**E**) The indicated GST-RABs were incubated with or without GST-TBK1 (1 hour at 30°C, with ATP), and reaction products were separated by Phostag-PAGE and immunoblotted with α-GST antibody. (**F**) Coomassie blue SDS-PAGE analysis of purified GST-RAB8A^{WT}, RAB8A^{S72A}, and RAB8A^{S111A} after purification from *E. coli*. (**G**) The indicated GST-RAB8A proteins were incubated with or without GST-TBK1 and analyzed as in (E).

to loss of GST-pS72-RAB7A phosphorylation by Phostag-PAGE (Fig. 4, E and F, and fig. S2C). We then incubated immobilized GST-RAB7A or GST-pS72-RAB7A with extracts from RAB7A$^{-/-}$ cells and examined the interaction with FLCN by immunoblotting (Fig. 4G). GST-pS72-RAB7A bound FLCN ~2.9-fold more efficiently than either GST-RAB7A or resin alone, which were similar in the level of FLCN bound (Fig. 4H). In an alternative approach, we purified a HA-FLCN/FLAG-FNIP1 complex by overexpression in 293T cells using α-FLAG resin (fig. S2D) and incubated equal amounts of complex with recombinant GST-RAB7A^{WT}, S72A, S72E, or the constitutively inactive GDP-locked T22N mutant. RAB7A^{S72E} displayed enhanced binding (about twofold) when compared with RAB7A^{WT} and S72A mutants (Fig. 4I). These data suggest that phosphorylation of S72 in RAB7A leads to a form of the protein that preferentially associates with the FLCN/FNIP1 complex. Previous studies indicate that DENN domain proteins that function as GEFs for individual RABs bind more tightly to the GDP-locked forms of the protein (*36*). We found that RAB7A^{T22N} bound poorly to

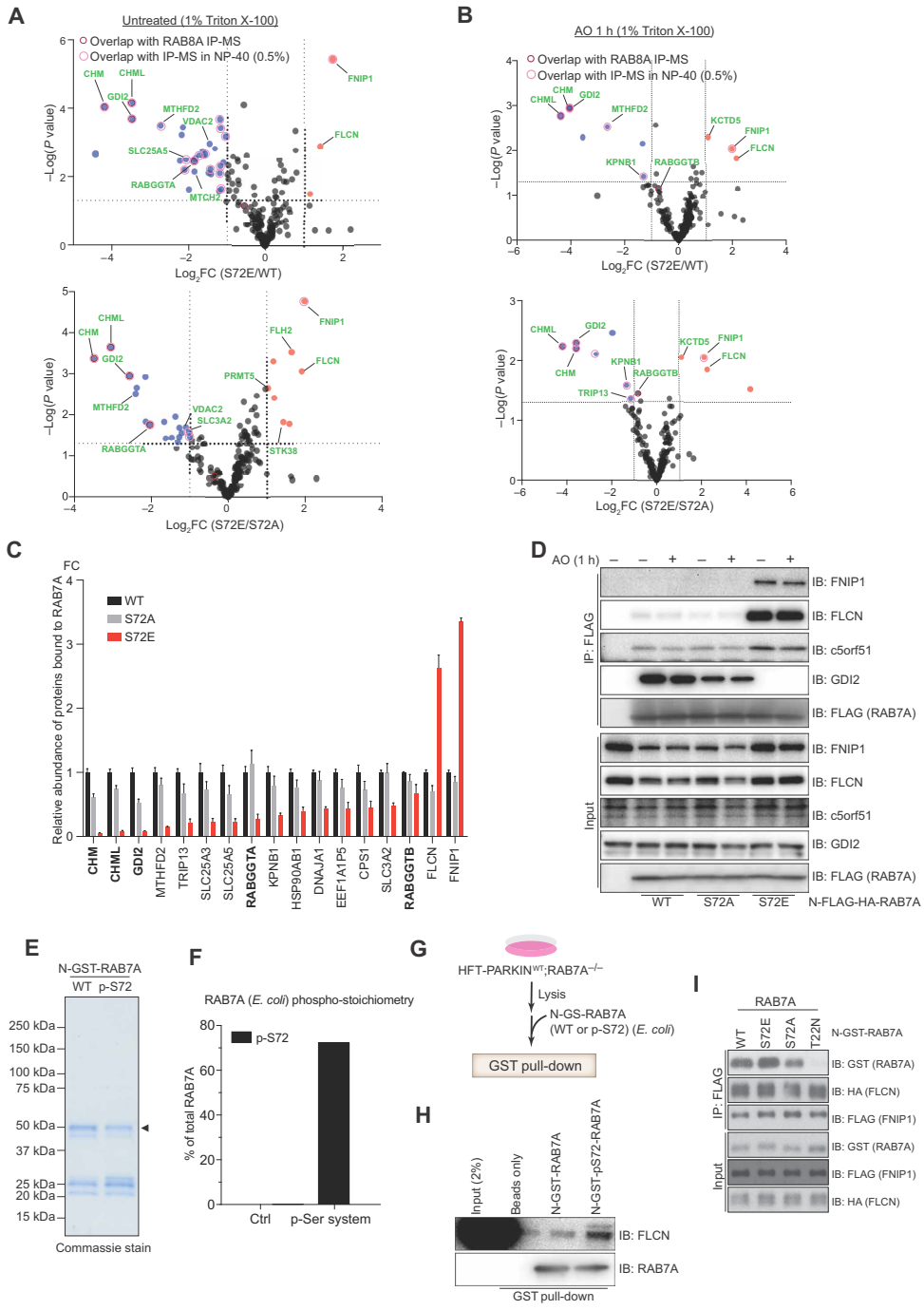

Fig. 4. Quantitative proteomic analysis of nonphosphorylatable and phosphomimetic RAB7A^{S72} reveals a phosphorylation-dependent interaction with FNIP1/FLCN. (**A**) Triton X-100 (1%) lysates from HFT PARKIN^{WT};RAB7A$^{-/-}$ cells reconstituted with FLAG-HA-RAB7A^{WT} or the S72A or S72E mutants (see Fig. 2B) were subjected to α-FLAG immunoprecipitation-MS in triplicate, and interacting proteins were quantified by TMT-based proteomics. Volcano plots of −qlog(*P* value) versus the $\log_2$FC of the indicated pairs of proteins for triplicate measurements are shown. (**B**) As in (A) but depolarized for 1 hour with AO. (**C**) Histogram of the relative abundance of selected proteins found in association with RAB7A^{WT} and either S72A or S72E mutants. Error bars represent SEM from biological triplicate measurements. (**D**) The indicated cell lines were left untreated or depolarized for 1 hour with AO, and α-FLAG immunoprecipitates were subjected to immunoblotting with the indicated antibodies. (**E**) GST-RAB7A and pS72-GST-RAB7A were made in *E. coli*. For pS72-GST-RAB7A, protein was made using the amber codon suppressor system in the presence of a tRNA system for activation of phospho-Ser (*35*). Both proteins were purified using glutathione (GSH)–Sepharose and separated by SDS-PAGE before Coomassie staining. (**F**) The stoichiometry of GST-RAB7A phosphorylation on S72 was measured using PRM proteomics and found to be ~70%. (**G**) Schematic for use of immobilized pS72-GST-RAB7A for binding to FLCN in cell extracts. (**H**) Immobilized GST-RAB7A, pS72-GST-RAB7A, or GSH-resin was incubated with cell extracts (4 hours at 4°C), and washed beads were subjected to SDS-PAGE and immunoblotting with either α-FLCN or α-RAB7A antibodies. Extract (2% of input) was run as a loading control. (**I**) HA-FLCN/FLAG-FNIP1 complexes (6 μg, purified from mammalian cells and immobilized on α-FLAG resin) were incubated with 20 μg of GST-RAB7A^{WT} or S72A, S72E, or T22N mutants (3 hours at 4°C). Washed resin was subjected to SDS-PAGE and immunoblotting with the indicated antibodies. Input proteins were similarly analyzed in parallel.

HA-FLCN/FLAG-FNIP1, which is inconsistent with FLCN-FNIP1 being a GEF for RAB7A. In addition, FLCN does not support GEF activity for RAB7 in vitro while being active for RAB35 (*23*). Given that GAP activity for FLCN-FNIP1 has been demonstrated for RAGC/D GTPase (*24*, *25*), we also directly tested this possibility. However, we were unable to detect GAP activity for either $RAB7A^{WT}$ or $RAB7A^{S72E}$ in vitro using FLCN-FNIP1 purified from 293T cells (fig. S2E) under conditions where FLCN is active as a GAP on RAGC/D GTPase (*24*, *25*).

Second, we found that $RAB7A^{S72E}$ displayed reduced association with GDI proteins, as well as components of the geranylgeranyltransferase (GGTase) complex (CHM, CHML, and RABGGTA), an effect not seen with $RAB7A^{S72A}$ (Fig. 4, A to C, and fig. S2, A and B). A similar reduction in association of these components was also seen previously with $RAB8^{S72E}$, mimicking phosphorylation by LRRK2 (*21*). Mitochondrial depolarization was shown previously to promote recruitment of RAB7A to damaged mitochondria based on immunofluorescence of the endogenous protein (*17*). Given that $RAB7A^{S72E}$ failed to associate with GDI proteins and the GGTase, it is expected to be defective in cycling through membrane-associated organelles (*21*, *28*). As anticipated (*17*), we found that a fraction of FLAG-HA-$RAB7A^{WT}$ expressed at near endogenous levels in HFT-$PARKIN^{WT}$;$RAB7A^{-/-}$ cells localize to puncta that frequently overlap with fragmented mitochondrial at 1.5 hours after depolarization, with Mander's coefficients of 0.62 (fig. S2, F and G). Similar results were found with FLAG-HA-$RAB7A^{S72A}$. In contrast, $RAB7A^{S72E}$ remained diffusely localized (fig. S2, F and G), potentially reflecting an inability to cycle through GDI and GGTase functions for membrane targeting. The inability of $RAB7A^{S72E}$ to be properly targeted to membranes as a result of the absence of cycling through GDI/GGTase complicates the interpretation of results with this mutant, and we therefore focused the remaining functional studies on the nonphosphorylatable $RAB7A^{S72A}$ mutant.

Nonphosphorylatable $RAB7A^{S72A}$ fails to recruit FLCN-FNIP1 to damaged mitochondria

We previously developed a biochemical method for examining enrichment of proteins, including cargo receptors, on mitochondria in response to depolarization (*33*, *37*). Briefly, mitochondria were rapidly isolated after depolarization, and mitochondrial extracts were subjected to immunoblotting. Using this assay, we found that the endogenous FLCN-FNIP1 complex is enriched on mitochondria 1 hour after depolarization in HFT-$PARKIN^{WT}$;$RAB7A^{-/-}$ cells reconstituted at endogenous levels with FLAG-HA-$RAB7A^{WT}$ (Fig. 5, A and B). Strikingly, in analogous experiments with nonphosphorylatable FLAG-HA-$RAB7A^{S72A}$, endogenous FLCN-FNIP1 recruitment was greatly diminished, suggesting that S72 RAB7A phosphorylation is required for FLCN-FNIP1 recruitment to mitochondria (Fig. 5, A and B). TOMM20 ubiquitylation as a readout of PINK1-PARKIN activation indicated that they are functional in FLAG-HA-$RAB7A^{S72A}$–expressing cells (Fig. 5A). To rigorously examine the requirement for $RAB7A^{S72}$ phosphorylation in this activity, we replaced S72 with Ala in the endogenous alleles of RAB7A in HFT-$PARKIN^{WT}$ cells using CRISPR-Cas9 (Fig. 5C). Two independent clones of these cells (B1 and C2) had equal levels of RAB7A protein in whole-cell extracts and displayed similar levels of TBK1 activation as well as TOMM20 ubiquitylation in response to mitochondrial depolarization, indicating that upstream signals are maintained (Fig. 5D). Again, we found that recruitment of FLCN and FNIP1 to mitochondria was defective in $RAB7^{S72A}$ knock-in cells, despite similar amounts of RAB7A proteins in the mitochondrial lysate (Fig. 5, E and F). Together, these data are consistent with the idea that RAB7A phosphorylation by TBK1 promotes FLCN-FNIP1 recruitment to depolarized mitochondria downstream of PINK1-PARKIN activation.

Defective mitophagy in cells expressing $RAB7A^{S72A}$

Previous studies indicate that cells lacking RAB7A are defective in mitophagic flux and early steps in autophagy (*17*, *18*). To examine whether RAB7A phosphorylation is required, we tested mitophagy in HFT-$PARKIN^{WT}$ cells harboring homozygous $RAB7A^{S72A}$ mutants using a previously established sensitive image-based assay using α-DNA antibodies (Fig. 6A) (*7*, *38*). As demonstrated previously, depolarization results in aggregation of fragmented mitochondria, followed by turnover over an extended time course, allowing the quantification of the number of cells harboring unaggregated, aggregated, or cleared mitochondria (*7*, *38*). With $PARKIN^{WT}$ induction, 42% of cells had aggregated mitochondria and 46% of cells had cleared their mitochondria at 32 hours after depolarization (Fig. 6A). In two independent $RAB7A^{S72A}$ cell clones, only 20% of cells had cleared mitochondria, and there was a concomitant increase in the number of cells with aggregated mitochondria, indicating a role for RAB7A phosphorylation in mitophagy (Fig. 6A). Reduced mitophagy rates were also observed in HFT-$PARKIN^{WT}$;$RAB7A^{-/-}$ cells reconstituted with FLAG-HA-$RAB7A^{S72A}$ when compared with FLAG-HA-$RAB7^{WT}$ reconstituted cells (fig. S3A). As shown below, the $RAB7A^{S72A}$ mutant did not affect rapid recruitment of PARKIN, suggesting the absence of an effect on early steps in the process.

As an independent measure of mitophagic turnover, we used TMT-based quantitative proteomics to examine protein content of purified lysosomes from $RAB7A^{WT}$ and $RAB7A^{S72A}$ cells 16 hours after depolarization (Fig. 6B and data file S5). Volcano plots of lysosomal proteomes from triplicate cell cultures revealed marked increases in the abundance of the 473 detected mitochondrial proteins in purified lysosomes in $RAB7A^{WT}$ cells relative to $RAB7A^{S72A}$ cells (Fig. 6C), consistent with a defect in trafficking of damaged mitochondria to lysosomes. As expected (*6*, *7*, *37*), mitophagy cargo receptors (CALCOCO2, SQSTM1, NBR1, and TOLLIP) were also enriched in lysosomes 16 hours after depolarization in $RAB7A^{WT}$ cells, but their levels were greatly reduced in cells expressing $RAB7A^{S72A}$ (Fig. 6D), again consistent with decreased delivery of cargo to lysosomes. In this experiment, peptides for OPTN were not detected. Control experiments revealed only modest effects of $RAB7A^{S72A}$ on lysosomal acidification, as measured by LysoTracker Red (fig. S3B).

FLCN promotes PARKIN-dependent mitophagy

Given the enhanced association of FLCN with pS72 or phosphomimetic RAB7A and the enrichment of FLCN-FNIP1 on mitochondria in response to depolarization (Figs. 4 and 5), we examined the involvement of FLCN in mitophagy. HFT-$PARKIN^{WT}$ or HFT-$PARKIN^{WT}$;$FLCN^{-/-}$ (with or without reconstitution with MSCV-FLAG-HA-FLCN) were depolarized, and mitophagic flux was measured after 32 hours (Fig. 6E). Loss of FLCN led not only to a 25% decrease in the proportion of cells with cleared mitochondria, but, unlike loss of RAB7A, also to a 22% increase in the fraction of cells with unaggregated mitochondria (Fig. 6E), suggesting multiple

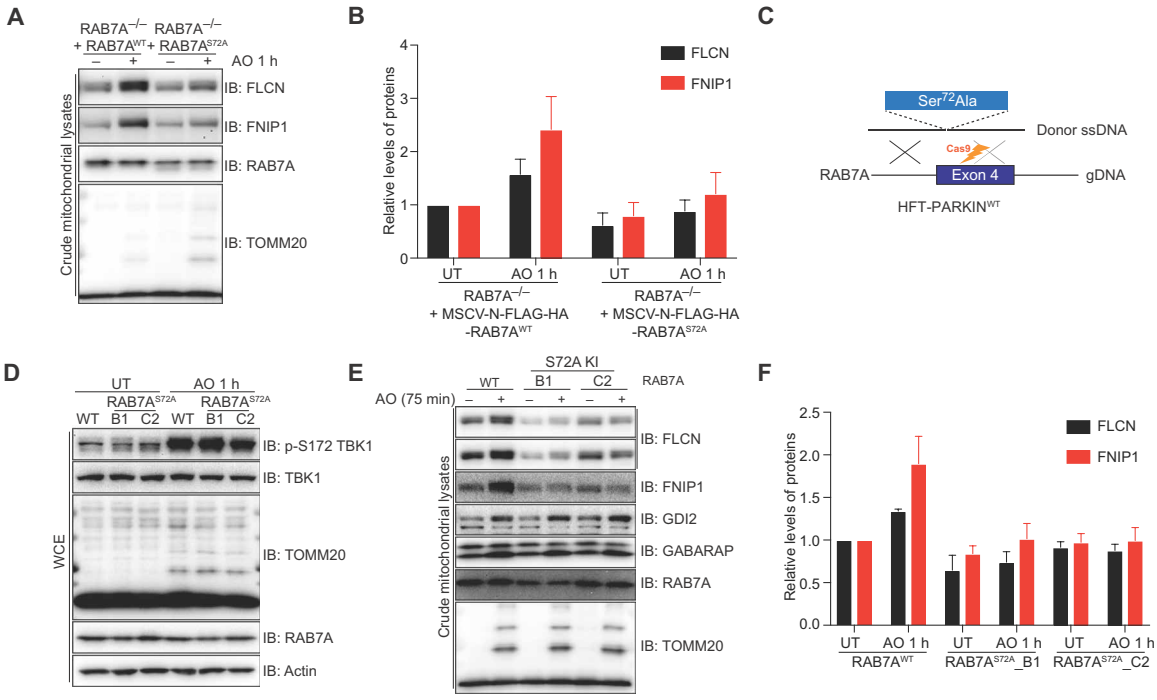

Fig. 5. RAB7A^{S72A} fails to support recruitment of FNIP1/FLCN to depolarized mitochondria. (**A**) The indicated HFT-PARKIN^{WT} cell lines were treated with DOX (16 hours) to induce PARKIN and depolarized with AO (1 hour), and mitochondrial extracts were subjected to SDS-PAGE and immunoblotting with the indicated antibodies. (**B**) Quantification of biological triplicate experiments as described in (A). Error bars represent SEM. (**C**) Schematic describing how S72 in RAB7A was replaced by Ala using CRISPR-Cas9. The replacement template used was single-stranded DNA containing S72A. (**D** and **E**) HFT-PARKIN^{WT} cell lines were treated with DOX (16 hours) to induce PARKIN and depolarized with AO for 1 hour, and either whole-cell lysates (D) or mitochondrial extracts (E) were subjected to SDS-PAGE and immunoblotting using the indicated antibodies. (**F**) Quantification of biological triplicate experiments as described in (B). Error bars represent SEM.

effects. Reconstitution with FLAG-HA-FLCN rescued these defects and actually increased mitochondrial clearance and decreased the fraction of cells with unaggregated mitochondria (Fig. 6E), likely reflecting the increased levels of FLCN in the rescued cells (fig. S3C). We found that PARKIN-dependent ubiquitylation of CISD1, MFN2, and TOMM20, as well as the accumulation of Ub chains on mitochondria, was reduced by approximately twofold in FLCN$^{-/-}$ cells and this was rescued by FLAG-HA-FLCN (fig. S3C), suggesting that the reduction in mitochondrial aggregation could reflect reduced rates of early steps in the pathway. Consistent with reduced substrate ubiquitylation and pS65-Ub in FLCN$^{-/-}$ cells, reduced PARKIN levels were observed on mitochondria from FLCN$^{-/-}$ cells relative to WT cells 1.5 hours after depolarization (fig. S3D).

Defective recruitment of ATG9A to damaged mitochondria in RAB7A^{S72A} cells

Available data suggest that multiple independent pathways support recruitment of autophagic machinery to cargo destined to encapsulation in an autophagosome and delivery to the lysosome. For example, cells lacking RAB7A accumulate ATG8, ULK1, and WIPI proteins on mitochondria in response to depolarization but fail to recruit ATG9A-positive vesicles (*17*). This has led to a model in which the ability to effectively convert ATG8 and ATG16L1-nucleated autophagosomes to structures capable of engulfing damaged mitochondria relies on recruitment of ATG9A-positive vesicles in a manner that is dependent on RAB7A (*17*). We found that ATG9A is enriched on purified mitochondria 2 hours after depolarization in RAB7A^{WT} cells, consistent with previous studies (*17*), but ATG9A enrichment was largely absent in RAB7A^{S72A} cells (Fig. 6F). In this experiment, the RAB7A^{S72A} mutation had no effect on the extent of TOMM20 ubiquitylation, the accumulation of pS65-Ub, TBK1 phosphorylation, or the accumulation of PINK1 and PARKIN on mitochondria, indicating the absence of an effect on upstream PINK1-PARKIN signaling (Fig. 6F). Moreover, enrichment of ATG8 proteins (LC3B and GABARAP), the phosphoinositide 3-kinase complex subunit BECN1 (Beclin1), and the WIPI2 protein that recognized phosphoinositide 3-phosphate on autophagic membranes were not affected in RAB7A^{S72A} mutants (Fig. 6F), consistent with previous studies (*17*). Thus, RAB7A^{S72A} mutants appear to be selectively defective in promoting recruitment of ATG9A vesicles and the FLCN-FNIP1 complex to damaged mitochondria, and the absence of these factors likely contributes to the reduced rates of mitophagy observed in RAB7A^{S72A} cells. In contrast, cells lacking FLCN still recruited ATG9 to mitochondria in response to depolarization (fig. S3D), suggesting independent functions for RAB7A and FLCN.

DISCUSSION

The emerging model for PINK1-PARKIN–driven mitophagy is that assembly of Ub chains on mitochondria supports the recruitment of Ub-binding cargo receptors typified by OPTN and SQSTM1 to the mitochondrial surface (*1*, *2*, *39*). In turn, these receptors are thought to facilitate assembly of autophagosomal membranes around the damaged mitochondria via interaction with ATG8 proteins using LIR motifs (*10*). TBK1 is found associated with cargo receptors and functions in a feed-forward loop to increase the Ub and ATG8

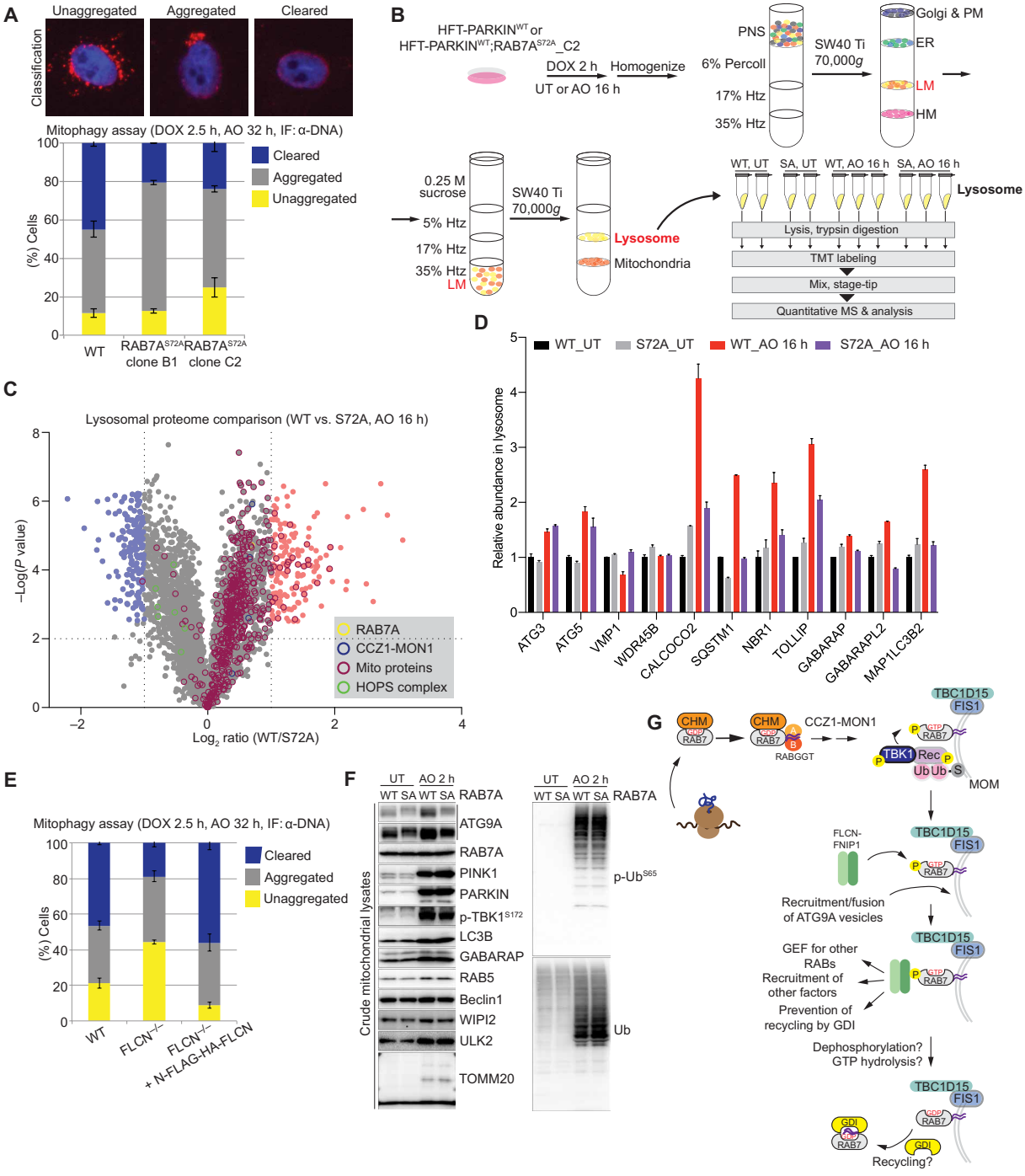

Fig. 6. Cells harboring nonphosphorylatable RAB7A are defective in mitophagic flux and fail to efficiently recruit ATG9A to damaged mitochondria. (**A**) Top: Example images of individual HFT-PARKIN^{WT} cells 32 hours after depolarization stained with α-DNA antibodies to detect unaggregated, aggregated, or cleared mitochondrial. Bottom: Histogram of the results of PARKIN-dependent mitophagy assays 32 hours after depolarization using the indicated cells and analyzed as in the top panel of (A). Error bars represent SEM from biological triplicate measurements, with >100 cells analyzed per replicate. Cells were treated with DOX for 2.5 hours to induce PARKIN before depolarization. (**B**) Schematic workflow for analysis of proteins enriched in lysosomes from cells expressing wild-type (WT) or S72A RAB7A. Extracts from the indicated cells were subjected to density centrifugation, and lysosomal fractions were subjected to 10-plex TMT using SPS-MS^3 analysis (*26*). (**C**) Volcano plot [–log(*P* value) versus $\log_2$FC (RAB7A^{WT}/RAB7A^{S72A})] of proteins present in the lysosomal fraction 16 hours after depolarization. Proteins in pink or blue represent proteins with $P < 0.05$ and $\log_2$FC of >1.5 or <–1.5, respectively. Mitochondrial proteins (based on MitoCarta2.0) are shown in dark red circles, while the location of RAB7A itself, the HOPS complex, and CCZ1-MON1 is shown in yellow, green, and blue circles, respectively. (**D**) Histogram of the relative abundance of selected mitophagy-related proteins in the lysosome based on the data in (C). (**E**) Mitophagy assays as in (A) for cells lacking FLCN with or without rescue with MSCV-FLAG-HA-FLCN. (**F**) The indicated cells were depolarized with AO for 2 hours, and mitochondria were purified before SDS-PAGE and immunoblotting with the indicated antibodies. SA, S72A. (**G**) Working model for TBK1-driven phosphorylation of RAB7A and downstream regulation of mitophagy. See text for details. ER, endoplasmic reticulum; HM, heavy mitochondria; LM, light mitochondria; PM, plasma membrane.

binding activity through phosphorylation of cargo receptors (*11*, *40*). Given that the synapse between mitochondrial membranes and growing autophagosomal membranes is likely a site of membrane fusion events as the autophagosome elongates, we thought it likely that TBK1 could function to regulate additional events through phosphorylation of additional targets in response to mitochondrial damage. Phosphoproteomic analysis of cells undergoing PINK1- and PARKIN-dependent mitophagy, combined with follow-up functional studies, revealed that S72 in RAB7A—a GTPase known to be involved in mitophagy (*17*, *18*)—is targeted directly by TBK1 in a manner that depends on Ub chain synthesis by PARKIN on damaged mitochondria. Thus, TBK1 can be viewed as a major regulator of events that bring about efficient recognition, capture, and disposal of damaged mitochondria.

Phosphorylation of RAB7A on S72 by TBK1 is interesting particularly in light of the fact that LRRK2 phosphorylates a distinct set of RABs on the homologous site within switch II, and this activity is markedly increased in the context of LRRK2 alleles found in Parkinson's disease (*21*, *22*). LRRK2 activity appears to be limited to a subset of RABs that have Thr at position 72 (or its equivalent), and it does not phosphorylate S72 in RAB7A (*21*). We found that TBK1 was unable to phosphorylate several RABs that are LRRK2 targets, suggesting that TBK1 may have specificity for RABs harboring Ser at this position or, alternatively, may have specificity for individual RABs. The major function thus far associated with phosphorylation of RABs by LRRK2 is loss of association with GDI, which effectively leads to increased RAB association with membranes in the context of activating LRRK2 alleles, thereby altering membrane fusion rates (*21*, *22*). We observed a similar effect with RAB7A in that the phosphomimetic RAB7A^{S72E} failed to interact with GDI, as noted previously (*41*), and GGTase, as assessed by quantitative proteomics. Consistent with this, RAB7A^{S72E} failed to be recruited to mitochondria in response to depolarization, suggesting that incorporation into membranes and/or recycling is needed for this response.

Unexpectedly, RAB7A^{S72E} displayed a marked increase, relative to either RAB7A^{WT} or RAB7^{S72A}, in the ability to associate with FLCN and FNIP1, leading to the hypothesis that RAB7A^{S72} phosphorylation is playing a positive role in this interaction. FLCN (which is mutated in the Birt-Hogg-Dubé cancer predisposition syndrome) and FNIP1 (or FNIP2) are known to form heterodimers (*42*), and both contain protein folds that largely superimpose on uDENN, cDENN, and dDENN domains (www.uniprot.org) (*23*). Classically, DENN domains are thought to act as GEFs for RABs (*36*), and FLCN has been reported to function as a GEF for RAB35 (but not RAB7) in vitro (*23*). However, the DENN domains in FLCN and FNIPs lack specific residues implicated in the GEF activity of DENN1B on RAB35 (*23*, *43*), raising questions about its mechanism of action. Previous studies suggest a bewildering array of interactions and activities for FLCN-FNIP complexes or FLCN alone, including GAP activity toward RAGC/D, where it functions as a regulator of mTOR (mammalian target of rapamycin) activation in response to amino acid depletion and is recruited to lysosomes through association with RAGA/B (*24*, *25*, *44*). Moreover, FLCN was reported to interact with adenosine 5′-monophosphate–activated protein kinase (AMPK), the ATG8 protein GABARAP, and several RABs (*42*, *45*, *46*). We validated interactions between FLCN-FNIP1 and RAB7A, and demonstrated that this association is enhanced by phosphorylation of RAB7A on S72 but is greatly reduced when RAB7A is in the GDP-bound form, which is inconsistent with a role as a GEF. We also failed to demonstrate GAP activity of FLCN-FNIP1 complexes on RAB7A in vitro (*42*). Previous studies suggest that the FLCN or DENN domain proteins may functionally link a GTP-bound RAB with either a target RAB for GDP-GTP exchange or a RAB effector (*44*, *47*).

Together, these data suggest a working model (Fig. 6G) wherein newly synthesized RAB7A is geranylgeranylated and can insert into cellular membranes. In response to mitochondrial depolarization and assembly of Ub chains by PARKIN, TBK1 and its associated Ub-binding cargo receptors are recruited to the MOM. In parallel, RAB7A is recruited to mitochondria through a poorly understood CCZ1-MON1–dependent pathway (*17*), which appears to be independent of S72 phosphorylation, as RAB7A^{S72A} is still recruited to depolarized mitochondria. Within the context of the MOM, activated TBK1 can phosphorylate a small pool of RAB7A on S72. We propose that this modification could result in multiple outcomes. First, we found that RAB7A^{S72E} in cells and pS72-RAB7A made in *E. coli* interact more efficiently with FLCN-FNIP1 complexes, and that FLCN-FNIP1 recruitment to mitochondria is deficient in cells expressing nonphosphorylatable RAB7A^{S72A}. This suggests that pS72-RAB7A may participate in the recruitment or retention of FLCN-FNIP1 on mitochondria through a direct interaction (Fig. 6G). Currently, we do not have evidence that FLCN-FNIP1 promotes GTP hydrolysis or GDP-GTP exchange for RAB7A, but it is possible that the association of FLCN-FNIP1 with pS72-RAB7A on mitochondria promotes GAP or GEF activity on other RABs locally or leads to recruitment of other effectors, as proposed for RAB34 and its effector RILP (*47*). Second, we validated the previous finding that ATG9A is recruited to damaged mitochondria and that this not only requires RAB7A, as previously reported (*17*, *18*), but also fails to occur in RAB7A^{S72A} mutants, indicating a positive role for RAB7A phosphorylation in ATG9A recruitment. However, ATG9A recruitment to mitochondria is largely unaffected in cells lacking FLCN, indicating that RAB7A-dependent recruitment of ATG9A does not occur through an FLCN intermediate (Fig. 6G). ATG9A-containing vesicles are recruited to sites of autophagosome formation and are thought to be a source of membranes for autophagosome assembly, although ATG9A is not itself incorporated into autophagosomes (*20*). We found that RAB7A^{S72E} poorly associates with GDI. Thus, phosphorylation of RAB7A^{S72} may reduce the rate of removal of RAB7A from membranes in the vicinity of damaged mitochondria until pS72-RAB7A is dephosphorylated by an as yet unknown phosphatase (Fig. 6G). In this regard, PTEN has been suggested to regulate RAB7A dephosphorylation in the context of epidermal growth factor receptor (EGFR) signaling through the endosome (*41*). Last, we also expect that RAB7A-GTP is acted upon by the MOM-associated GAPs TBC1D15/17 to facilitate removal by GDI (*16*, *17*). Further studies are required to elucidate the precise mechanisms by which phosphorylation of RAB7A by TBK1 controls discrete steps in mitophagy and to understand whether analogous mechanisms are at play in other TBK1–cargo receptor–driven autophagy pathways.

MATERIALS AND METHODS

Cell culture and gene editing

HFT PARKIN$^{WT/S65A}$ cells as well as cells lacking either PINK1 or TBK1 were generated as previously described (*7*, *38*). Cells were grown in Dulbecco's modified Eagle's medium (DMEM) with 10% fetal bovine serum (FBS) and hygromycin (200 μg/ml). To induce

PARKIN expression, cells were treated with 0.5 μM DOX as indicated. Cells were then either left untreated or depolarized with a mixture of antimycin A (10 μM) and oligomycin A (5 μM) (Sigma) (referred to as AO) for the indicated time period. To obtain whole-cell extracts, at each time point, cells were washed twice with ice-cold phosphate-buffered saline (PBS) and lysed in lysis buffer [50 mM tris-HCl (pH 7.5), 150 mM NaCl, 0.5% (v/v) NP-40 (or 1% Triton X-100), and protease/phosphatase inhibitor tablets (Roche)]. Mitochondria were purified as described previously (*37*) and lysed in lysis buffer.

Cas9-mediated gene editing for the creation of RAB7A and FLCN null alleles was performed using the guide sequence targeting exons containing the start codon (RAB7A: exon 2: 5′-GTCATCCTTCAAACTAAAGG-3′; FLCN: exon 5: 5′-TGCCACTTCTGCGAGCTCCA-3′) (*37*). To generate N-terminal EGFP tagging at TBK1 genomic locus, single-guide RNA (sgRNA) targeting the TBK1 start codon located within exon 2 (5′-ATTAGAAGTGCTCTGCATCT-3′) was simultaneously transfected with a donor plasmid containing 500–nucleotide (nt)–long homology arms upstream and downstream of the TBK1 start codon with the EGFP fragment upstream and in-frame with the TBK1 start codon. Introduction of the RAB7A^{S72A} mutation into the genome was achieved by cotransfecting the guide sequence (exon 4: 5′-CAGGAACGGTTCCAGTCTCT-3′) targeting near S72 in RAB7A and a single-strand DNA harboring the S72A mutation with 75-nt-long homology arm on each side as a donor for repair by homologous recombination. To validate gene edition, target regions were polymerase chain reaction (PCR) amplified and sequenced.

To generate RAB7A as well as other RAB GTPase mutants, QuikChange mutagenesis was performed on the WT constructs by using the KOD Hot Polymerase (EMD Millipore) followed by Dpn 1 digestion. For stable expression of RAB7A variants as well as FLCN in cells, MSCV retroviral constructs containing the indicated open reading frames were packaged into virus used to infect the indicated cells, and stable cell lines were selected in puromycin (1 μg/ml), as described previously.

Antibodies, immunofluorescence, and image analysis

The following antibodies were used in this study: α-MFN2 ([NIAR164], Abcam), α-TOMM20 (sc-11415, Santa Cruz Biotechnology), α-PARKIN (sc-32282, Santa Cruz Biotechnology and [EPR5024(N)], Abcam), α-Ub (Dako), α-HA (11867423001, Roche), α-TBK1 (3013S, Cell Signaling Technology), α-pS172 TBK1 (5483P, Cell Signaling Technology), α-GST (2625P, Cell Signaling Technology), α-actin (sc-69879, Santa Cruz Biotechnology), α-RAB7A (9367S, Cell Signaling Technology), α-PINK1 (AW5456-U400, Abgent), α-HA (53363, BioLegend), α-FLAG (F1804-200UG, Sigma), α-pS65-Ub (ABS1513, EMD Millipore), α-LC3B (2775S, Cell Signaling Technology), α-GABARAP (GTX132657, Genetex), α-CISD1 (16006-1-AP, Proteintech), α-FLCN (3697S, Cell Signaling Technology), α-FNIP1 (MABS1717, EMD Millipore), α-c5orf51 (bs-9484R, Bioss), α-GDI2 (AP13787c, Abgent), α-ATG9A (ab108338 , Abcam), α-ULK2 (GTX111476, Genetex), α-RAB5 (3547S, CST), α-Beclin1 (3495, Cell Signaling Technology), and α-WIPI2 (MCA5780GA, Bio-Rad).

For immunofluorescence, the indicated cells were left untreated or incubated with AO for the indicated time period. Cells were then fixed with 4% paraformaldehyde, permeabilized with 0.2% Triton X-100, blocked with 1% bovine serum albumin, and subjected to immunostaining using indicated antibodies as previously described (*7*). Hoechst dye was used to stain the nucleus. To image cells, a Yokogawa CSU-X1 spinning disc confocal lens on a Nikon Ti-E inverted microscope equipped with a 100-Å Plan Apo NA (numerical aperture) 1.4 objective lens in the Nikon Imaging Center at Harvard Medical School was used. Mander's colocalization coefficient was obtained by using the Fiji Coloc 2 plugin, as described previously (*7*).

For mitophagy assays, each cell line was treated with DOX (0.5 μM to induce PARKIN expression) for 2.5 hours, washed, and then treated with AO, as indicated. After 32 hours of AO treatment, cells were fixed, permeabilized, blocked, and immunostained with α-DNA antibody followed by Hoechst staining as above. Images were acquired as described above. For quantification, >100 cells were counted for each replicate on the basis of the classification of unaggregated mitochondria, aggregated mitochondria, and cleared mitochondria in biological triplicate.

TBK1 phosphoproteomics

To perform TBK1 phosphoproteomic screens, HFT-PARKIN^{WT} cells with or without TBK1 were treated with DOX for 6 hours to induce PARKIN expression and then incubated with AO as indicated. All downstream proteomic steps were performed exactly as described previously (*48*). Following harvest, cells were lysed in denaturing lysis buffer [8 M urea, 50 mM NaCl, 50 mM EPPS [4-(2-hydroxyethyl)-1-piperazinepropanesulfonic acid] (pH 8.0), and protease and phosphatase inhibitor tablets (Roche)], and 10 mg of lysates was used for each condition. Lysates were then subjected to reduction [10 mM tris(2-carboxyethyl)phosphine (TCEP)] and alkylation (15 mM iodoacetamide) followed by methanol-chloroform extraction. Proteins were digested overnight at 37°C with Lys-C and trypsin [10 mM tris-Cl (pH 8.5) and 1 M urea]. Digests were acidified with an equal volume of 5% (v/v) formic acid (FA) to a pH of ~2 for 30 min and loaded on Sep-Pak (Waters, C18) for desalting. Dried peptides were resuspended in a buffer [2 M lactic acid, 50% acetonitrile (ACN), and 0.1% trifluoroacetic acid (TFA)], incubated with 50 mg of immobilized TiO_2 (1400B500, GL Sciences) for 1.5 hours at room temperature, washed, and eluted with elution buffer [50 mM HK_2PO_4 (pH 10)] followed by acidification with FA to a final concentration of 1% (v/v). Peptides were subjected to the desalting procedure using the Sep-Pak as above, labeled with 10-plex TMT reagents (Thermo Fisher Scientific, Rockford, IL), mixed, and desalted with a C18 StageTip (packed with Empore C18; 3M Corporation).

Phosphopeptide samples were analyzed on a Fusion Lumos mass spectrometer (Thermo Fisher Scientific, San Jose, CA) coupled to a Proxeon EASY-nLC 1200 liquid chromatography (LC) pump (Thermo Fisher Scientific). Peptides were separated on a 100–μm–inner diameter microcapillary column packed with 35 cm of Accucore C18 resin (2.6 μm, 150 Å; Thermo Fisher Scientific). For each analysis, we loaded approximately 2 μg onto the column. Peptides were separated using a 2-hour gradient of 3 to 25% ACN in 0.125% FA with a flow rate of ~500 nl/min. Each analysis used a synchronous precursor selection (SPS)–MS^3–based TMT method (*26*). Before starting our analysis, we perform two injections of trifluoroethanol to elute any peptides that may be bound to the analytical column from previous injections to limit carryover. The scan sequence began with an MS^1 spectrum [Orbitrap analysis; resolution of 120,000 at 350 to 1400 Thomson (Th), automatic gain control (AGC) target of 5×10^5, and maximum injection time of 100 ms]. The top 10 precursors were then selected for MS^2/MS^3 analysis. MS^2 analysis consisted of collision-induced dissociation (CID), quadrupole ion trap analysis, AGC target of 2×10^4, normalized collision energy (NCE)

of 35, q value of 0.25, maximum injection time of 120 ms, and isolation window at 0.7. Following acquisition of each MS^2 spectrum, we collected an MS^3 spectrum in which multiple MS^2 fragment ions are captured in the MS^3 precursor population using isolation waveforms with multiple frequency notches. MS^3 precursors were fragmented by high-energy collision-induced dissociation (HCD) and analyzed using the Orbitrap (NCE of 65, AGC target of 1.5×10^5, maximum injection time of 150 ms, and resolution of 50,000 at 400 Th). For MS^3 analysis, we used charge state–dependent isolation windows. For charge state $z = 2$, the isolation window was set at 1.3 Th, for $z = 3$ at 1 Th, for $z = 4$ at 0.8 Th, and for $z = 5$ at 0.7 Th.

Mass spectra were processed using a Sequest-based pipeline with a human UniProt database, as described (*49*). This database was concatenated with one composed of all protein sequences in the reversed order. Searches were performed using a 20 ppm (parts per million) precursor ion tolerance for total protein level analysis. The product ion tolerance was set to 0.9 Da. TMT tags on lysine residues and peptide N termini (+229.163 Da) and carbamidomethylation of cysteine residues (+57.021 Da) were set as static modifications, while oxidation of methionine residues (+15.995 Da) and phosphorylation of Ser, Thr, and Tyr (+79.966 Da) were set as variable modifications.

Peptide-spectrum matches (PSMs) were adjusted to a 1% false discovery rate (FDR), and PSM filtering was performed using a linear discriminant analysis (LDA), as described previously (*49*), while considering the following parameters: XCorr, ΔCn, missed cleavages, peptide length, charge state, and precursor mass accuracy. For TMT-based reporter ion quantitation, we extracted the summed signal-to-noise ratio for each TMT channel and found the closest matching centroid to the expected mass of the TMT reporter ion. For protein-level comparisons, PSMs were identified, quantified, and collapsed to a 1% peptide FDR and then collapsed further to a final protein-level FDR of 1%, which resulted in a final peptide-level FDR of <0.1%. Moreover, protein assembly was guided by principles of parsimony to produce the smallest set of proteins necessary to account for all observed peptides.

Proteins were quantified by summing reporter ion counts across all matching PSMs, as described previously (*26*). PSMs with poor quality, MS^3 spectra with more than eight TMT reporter ion channels missing, MS^3 spectra with TMT reporter summed signal-to-noise ratio of less than 100, and having no MS^3 spectra were excluded from quantification. Each reporter ion channel was summed across all quantified proteins and normalized assuming equal protein loading of all 10 samples. Student's t tests were used to determine statistical significance between each treatment and controls for each cell line, as well as to compare protein abundance levels between cell lines. In all cases, $P < 0.05$ was considered statistically significant. A second threshold based on a $\log_2$FC of greater than 1.5-fold or less than −1.5-fold was chosen to focus the data analysis on a small set of proteins with the largest alterations in abundance. Protein quantification values were exported for further analysis in Microsoft Excel. Each reporter ion channel was summed across all quantified proteins and normalized to assume equal protein loading of all 10 samples across the 10-plex TMT. To determine total protein abundance, 100 μg of whole-cell lysates was digested with Lys-C and trypsin as above in 200 mM EPPS (pH 8.5), labeled with 10-plex TMT, mixed, and desalted with a C18 StageTip before SPS-MS^3 analysis on an Orbitrap Fusion instrument.

PINK1-PARKIN pathway mitochondrial phosphoproteomics

To examine the phosphoproteome of mitochondria in response to mitochondrial depolarization, biological duplicate cultures of HFT-$PARKIN^{WT}$ or S65A mutant cells, or HFT-$PARKIN^{WT}$;$PINK1^{-/-}$ cells, were depolarized for the indicated times, and mitochondria were isolated and digested as described (*33*). The flow-through from Kgg-enriched samples was acidified and subjected to Sep-Pak (Waters, C18) for desalting. Samples were resuspended in 80% ACN/0.1% TFA solution, and phosphopeptides were enriched using IMAC magnetic agarose beads (Ni-NTA, catalog no. 36111, Qiagen). Enriched peptides were subjected to Sep-Pak for desalting, resuspended in 100 μl of 0.1 M EPPS/20% ACN (pH 8.2), and labeled with TMT reagent for 1 hour at room temperature before quenching with 5 μl of 5% hydroxylamine. Labeled peptide was acidified to 0.1% TFA (pH ~2 to 3), and the Pierce High pH Reversed-Phase Peptide Fractionation Kit was used to collect 12 fractions and recombined for a total of 6 fractions before desalting and subsequent LC–tandem mass spectrometry (LC-MS/MS) processing.

MS data were collected on an Orbitrap Fusion Lumos mass spectrometer in line with a Proxeon NanoLC-1200 UHPLC. The 100-μm capillary column was packed with 35 cm of Accucore 150 resin (2.6 μm, 150 Å; Thermo Fisher Scientific). Samples were separated with a gradient consisting of 3 to 23% (ACN; 0.1% FA) over 150 min at ~550 nl/min. Each analysis used the MultiNotch SPS-MS^3–based TMT method (*26*) to reduce ion interference compared to MS^2 quantification. The scan sequence began with $FTMS^1$ spectra (resolution of 120,000, mass range of 400 to 1400 m/z, AGC target of 5×10^5, and maximum injection time of 100 ms). Precursors for MS^2 analysis were selected using a Top10 method. Precursors were filtered according to charge state ≥2 and ≤6. Monoisotopic peak assignment was used, and previously interrogated precursors were excluded using a dynamic window (90 s ± 7 ppm). Minimum intensity to trigger an MS^2 scan was 2×10^4. MS^2 precursors were isolated using the quadrupole (0.7-Th window) and analyzed in the Orbitrap ($FTMS^2$) at 30,000 resolution at 200 Th, with an AGC target of 5×10^4 and a maximum injection time of 118 ms. Precursors were fragmented by CID at a collision energy of 35% and an activation q value of 0.25. Multistage activation was triggered for neutral loss mass of 97.9763. Following acquisition of each MS^2 spectrum, an SPS-MS^3 scan was collected on the top 10 most intense ions in the MS^2 spectrum (*26*). MS^3 precursors were fragmented by HCD and analyzed using the Orbitrap (NCE of 55, AGC target of 3×10^5, maximum injection time of 250 ms, and resolution of 50,000 at 200 Th).

Database searching included all entries from the Human Reference Proteome (May 2017) and an in-house list of contaminants. This database was concatenated with one composed of all protein sequences in the reversed order. Searches were performed using the Comet search engine (2014.02 rev. 2) using a 20-ppm precursor ion tolerance, and the product ion tolerance was set to 0.03 Da. Peptide's N/C terminus was required to have Lys-C/trypsin specificity [1 1 KR], allowing up to three missed cleavages. TMT tags on lysine residues and peptide N termini (+229.163 Da) and the carbamidomethylation of cysteine residues (+57.021 Da) were set as static modifications, while the oxidation of methionine residues (+15.995 Da) was set as a variable modification. For phosphorylation analysis, deamidation (+0.984) on asparagine and glutamine and phosphorylation (+79.966) on serine and threonine were set as variable modifications. PSMs were adjusted to a 1% FDR, PSM filtering was performed using an LDA, and phosphorylation site localization was determined

using the Ascore algorithm, as described previously (*49*). Ascore is a probability-based approach for high-throughput protein phosphorylation site localization. Specifically, a threshold of 13 corresponded to 95% confidence in site localization. For quantification, reporter ion counts were summed across all matching PSMs using an in-house software (*49*). Briefly, a 0.003-Th window around the theoretical *m*/*z* value of each reporter ion was scanned for ions, and the maximum intensity nearest the theoretical *m*/*z* was used. Reporter ion intensities were adjusted to correct for the isotopic impurities of the different TMT reagents according to the manufacturer's specifications. MS^3 spectra with TMT reporter summed signal-to-noise ratio of <150 or isolation purities of <50% were excluded from quantitation (*26*). The extracted signal-to-noise measurements of peptides were then normalized to the corresponding protein level previously measured from the total mitochondrial proteome (*33*). Individual ratios to HFT-$PARKIN^{WT}$ untreated cells were calculated, and values were imported into Perseus (version 1.6.1.3) (*50*) for downstream statistical processing. *T* tests with Welch's correction for unequal variances were performed with the following parameters (S0 = 1), and permutation-based FDR correction to 1% was applied to correct for multiple test correction. Results from the statistical analysis were then exported and plotted as volcano plots.

In vitro kinase assays

RAB GTPases were expressed in *E. coli* as GST fusion proteins and purified by affinity pull-down on GSH-Sepharose. Briefly, GST fusion RAB GTPase–transformed bacterial cells were grown in Overnight Express Instant TB Medium (EMD Millipore) following the manufacturer's instruction, and the bacterial cell pellet was lysed in lysis buffer [50 mM tris (pH 7.5), 150 mM NaCl, 1% Triton X-100, 1 mM EDTA, 1 mM EGTA, 0.1% β-mercaptoethanol, and protease/phosphatase inhibitor tablet (Roche)]. Cleared lysates after centrifugation were incubated with the GSH-Sepharose (Gold Biotechnology) for 1 hour, washed, and eluted with 20 mM reduced GSH (G4251, Sigma). Three micrograms of purified GST fusion proteins was then subjected to the SDS-PAGE to determine their purity.

To perform in vitro kinase assays, the indicated GST-RAB GTPase (2 μM) was incubated with 0.2 μM TBK1 (~1.12 U) (purified from Sf21 insect cells, Ubiquigent #66-0016-050) in reaction buffer [50 mM tris-Cl (pH 7.5), 0.1 mM EGTA, 10 mM $MgCl_2$, and 2 mM dithiothreitol (DTT)]. Assays were initiated by adding ATP to a final concentration of 0.1 mM. Reactions were terminated after 60 min at 30°C by the addition of 4× lithium dodecyl sulfate (LDS) sample buffer (NP0008, Thermo Fisher Scientific) to a final concentration of 1× LDS, heated for 5 min at 75°C, and separated by either SDS-PAGE or Phostag-PAGE. Protein gels were then subjected to either Coomassie blue staining or immunoblotting.

PRM of pS172-TBK1 and pS72-RAB7A

For PRM, GFP-tagged TBK1 was immunoprecipitated from HFT-$PARKIN^{WT}$ with or without PINK1. Cells were washed twice with ice-cold PBS and lysed by sonication in lysis buffer. Lysates were cleared by centrifugation at 20,000*g* for 15 min at 4°C. The cleared supernatant was incubated with 30 μl of GFP-Trap (ChromoTek, gtma-10) for 4 hours at 4°C, and the beads were washed three times with ice-cold lysis buffer and three times with ice-cold PBS. Two elutions with 150 μl of 6 M GnHCl for 5 min at 65°C were performed. For PRM, FLAG-tagged RAB7A was immunoprecipitated from HFT-$PARKIN^{WT}$;$RAB7A^{-/-}$ stably expressing MSCV-FLAG-HA-RAB7A. Cells were washed twice with ice-cold PBS and lysed, the cleared supernatant was incubated with 30 μl of α-FLAG magnetic beads (Sigma) for 4 hours at 4°C, and the beads were washed three times with ice-cold lysis buffer and three times with ice-cold PBS. Two elutions with 150 μl of 3×FLAG peptide (125 μg/ml) for 10 min at 25°C were performed. Samples were then reduced (5 mM TCEP) and alkylated (20 mM chloroacetamide) before trichloroacetic acid precipitation. Samples were digested first with Lys-C [in 100 mM tetraethylammonium bromide (pH 8.5) and 10% (v/v) ACN] for 2 hours at 37°C, followed by the addition of trypsin, and further digested for 6 hours at 37°C. Digests were acidified with an equal volume of 5% (v/v) FA to a pH of ~2, dried down, and resuspended in 1% (v/v) FA. Samples were then resuspended in 1% (v/v) FA and analyzed by PRM as described previously (*37*) but with several modifications. A collection of four heavy labeled TBK1 reference peptides (^{163}ELEDDEQFV**S**LYGTEEYLHPD*M***Y**ER^{187} phosphorylated at Ser^{172} and with methionine oxidized and ^{144}VIGEDGQS**V**YK^{154}, ^{242}PSGAISG**V**QK^{251}, and ^{647}YQEYTNELQETL**P**QK^{661}) was produced at Cell Signaling Technology and quantified by amino acid analysis, and a collection of two heavy labeled RAB7 reference peptides (^{70}FQ**S**LGVAFY**R**^{79} phosphorylated or not at Ser^{172}) was produced (0.1 mg) at SynPeptide Co. Ltd (underlined residue is phosphorylated, and bold amino acid is heavy). Heavy reference peptides from working stocks [in 1% (v/v) FA] were diluted into the digested sample [in 1% (v/v) FA] to be analyzed at a final concentration predetermined for individual peptide. Samples and heavy reference peptides were oxidized with 0.05% hydrogen peroxide for 20 min, subjected to C18 StageTip (packed with Empore C18; 3M Corporation), and resuspended in 1% (v/v) FA/5% ACN. Experiments were performed in triplicate, and MS data were collected sequentially by LC/MS on a Q Exactive mass spectrometer (Thermo Fisher Scientific) coupled with a FAMOS autosampler (LC Packings) and an Accela600 LC pump (Thermo Fisher Scientific). Peptides were separated on a 100–μm–inner diameter microcapillary column packed with ~0.5 cm of Magic C4 resin (5 μm, 100 Å; Michrom Bioresources) followed by ~20 cm of Accucore C18 resin (2.6 μm, 150 Å; Thermo Fisher Scientific). Peptides were separated using a 35-min gradient of 5 to 27% ACN in 0.125% FA with a flow rate of ~300 $nl \cdot min^{-1}$. The scan sequence began with an Orbitrap full MS^1 spectrum with the following parameters: resolution of 70,000, scan range of 200 to 1000 Th, AGC target of 1×10^6, maximum injection time of 250 ms, and profile spectrum data type. This scan was followed by targeted MS^2 scans selected from a scheduled inclusion list. Each targeted MS^2 scan consisted of HCD with the following parameters: resolution of 17,500, AGC target of 5×10^4, maximum injection time of 200 ms, isolation window of 1 Th, NCE of 20, and profile spectrum data type. Raw files were searched, and precursor and fragment ions were quantified using Skyline version 3.5 (https://skyline.ms), as described (*37*). Data generated from Skyline were exported into an Excel spreadsheet and Prism for further analysis. Total TBK1 was determined as the average of the total TBK1 calculated from all three unmodified peptides and total RAB7A from the average of the S72 locus (S72 + pS72).

Expression and purification of phosphorylated proteins

To prepare site-specific phosphorylated RAB7A, we used a suppressor tRNA system in bacteria, allowing for direct incorporation of phosphoserine at a desired residue position as described previously (*35*). Briefly, the human RAB7A open reading frame fused to His6-GST

at its N terminus was mutated by PCR to replace the S72 with an Amber stop codon (TAG). 6×His-GST-RAB7A constructs were then subcloned in the pCRT7-NT-Topo-tetR/pLtetO Amp vector (52053, Addgene) by Gibson assembly. C321.ΔA strains (ΔmutS:zeo, ΔtolC, Δbla:tolC, and SerB-/ΔSerB) were cotransformed with the pCRT7 plasmid of interest and pKD-SepRS9-EFSep21-4xtRNA$^{Sep\text{-}A37}$ (SepOTS λ), and selection, growth, and induction were performed as described (*35*). The cells were collected and lysed in 50 mM Hepes (pH 7.5), 250 mM NaCl, 50 mM NaF, 270 mM sucrose, 0.03% Brij-35, 15 mM imidazole, 0.25 mM TCEP, and 1 mM AEBSF [4-(2-aminoethyl) benzenesulfonyl fluoride hydrochloride]. 6×His-GST-RAB7A and specific phosphoforms were affinity purified by using GSH-Sepharose resin as above.

SDS-PAGE, Phostag SDS-PAGE, and Western blotting

For SDS-PAGE, indicated cells were lysed in lysis buffer described above. Forty micrograms of whole-cell lysates (or 20 μg for purified mitochondrial lysates) was then loaded onto the SDS-PAGE and subjected to electrophoresis. For Phostag-PAGE, Phostag acrylamide (300-93523, Wako) was added to the 6% SDS–acrylamide gel mixture as suggested by the manufacturer. After electrophoresis, gels were transferred to polyvinylidene difluoride membrane and subjected to immunoblotting with indicated antibodies. To estimate differences in protein abundance by immunoblotting, we used a charge-coupled device camera in the M (Protein Simple) imager and relative summed pixel intensities were determined using ImageJ.

Purification of the FLCN-FNIP1 complex

To generate the FLCN-FNIP1 complex, 1 million FreeStyle 293 cells were inoculated in 2 liters of FreeStyle medium. Twenty-four hours later, cells were transfected using polyethylenimine (PEI) with 600 μg of FLAG-FNIP1 plasmid and 1.5 mg of HA-FLCN plasmid. Thirty-six hours after transfection, cells were spun down and washed once with PBS and lysed in 100 ml of Triton lysis buffer (TLB) [40 mM Na-Hepes (pH 7.4), 100 mM NaCl, 2 mM $MgCl_2$, 100 μM ATP, 10 mM $Na_4P_2O_7$, 10 mM Na β-glycerol phosphate, 1% Triton, and two tablets of protease inhibitor cocktail]. After centrifugation at 40,000*g* for 30 min, 4 ml of FLAG-M2 beads was added to the lysate. The FLCN-FNIP1 complex was immunoprecipitated for 3 hours at 4°C. The resin was then packed into a column and washed with 10 column volumes of TLB, followed by 20 column volumes of TLB supplemented with 300 mM NaCl. The resin was buffer exchanged into CHAPS buffer (CB) [40 mM Na-Hepes (pH 7.4), 150 mM NaCl, 2 mM $MgCl_2$, and 0.1% CHAPS] before elution with 3 × FLAG peptide (1 mg/ml) dissolved in CB. The eluent was concentrated using a 100-kDa molecular weight cutoff filter and spun at 100,000*g* for 30 min to remove any aggregates in preparation for fast protein LC. To improve the purity, the FLCN-FNIP1 complex was loaded onto a HiLoad 16/60 Superdex 200 gel filtration column pre-equilibrated in gel filtration buffer (GFB) [50 mM Na-Hepes (pH 7.4), 150 mM NaCl, 2 mM $MgCl_2$, 2 mM DTT, and 0.1% CHAPS]. The peak corresponding to FLCN-FNIP1 was collected, flash frozen in GFB supplemented with 10% glycerol, and stored at −80°C.

In vitro binding assay

To test the binding between FLCN-FNIP1 and various RAB GTPases, 6 μg of FLAG-tagged FLCN-FNIP1 was incubated with 20 μg of GST-tagged RAB protein in 1 ml of assay buffer (AB) [50 mM Na-Hepes (pH 7.4), 150 mM NaCl, 2 mM $MgCl_2$, 2 mM DTT, 100 μM GppNHp (guanosine 5′-[β,γ-imido]triphosphate), and 1% Triton]. The mixture was immunoprecipitated with 30 μl of FLAG-M2 beads for 3 hours at 4°C. The resin was washed once with AB and three times with AB supplemented with 250 mM NaCl, before the bound protein was stripped with 100 μl of 2× SDS gel loading buffer. The immunoprecipitant was analyzed using Western blot.

Single-turnover GTP hydrolysis assay

To determine the GTP hydrolysis rate of the RAB GTPase in the absence or presence of FLCN-FNIP1 under single-turnover conditions, 1 μM of RAB7A^{WT} or RAB7A^{S72E} was incubated with 1 nM [γ-^{32}P]GTP in the absence or presence of 2 μM FLCN-FNIP1. The reaction was carried out at 37°C in GTPase buffer [50 mM Na-Hepes (pH 7.4), 100 mM KOAc, 2 mM $MgCl_2$, 2 mM DTT, and 0.1% CHAPS]. Aliquots of the reaction mixture were taken at different time points and quenched using 0.75 M KH_2PO_4 (pH 3.3). The time points were applied to cellulose 300 PEI thin-layer chromatography (TLC) plates and expanded in TLC buffer (1 M FA and 0.5 M LiCl) for 20 min. The plates were dried and imaged with a phosphorimaging screen. The intensities of the radioactive signals were read out by a Typhoon scanner and quantified using the ImageQuant software, and the fraction of hydrolyzed GTP was reported.

Lysosomal purification and proteomic analysis

Cells expressing either RAB7A^{WT} or S72A were grown to 80 to 90% confluency, treated with DOX for 2.5 hours to express PARKIN, washed, and incubated with AO for 15 hours as above. For each sample, ten 15 cm × 2.5 cm (*D* × *H*) plates were used, and all steps were carried out with ice-cold reagents at 4°C. Lysosomal purification was performed following previously established protocol with minor modification (*51*). Cells were washed two times with PBS and carefully detached in PBS containing protease inhibitors (Sigma) (2 to 3 ml per plate) by using a cell lifter and transferred to tubes. Plastic Pasteur pipettes were used to handle cells and cell fractions at all steps of the experimental procedure. Cells were centrifuged at 500*g* for 5 min, and the supernatant was discarded and washed in isolation buffer (IB) [0.25 M sucrose, 10 mM Hepes (pH 7.4), 1 mM EDTA, and protease inhibitors]. Cells were centrifuged again at 500*g* for 5 min, and supernatant was discarded and resuspended in 3 to 4 ml of IB. Cells were homogenized with 15 to 20 strokes using a dounce-type homogenizer/Teflon pestle (Thomas Scientific). The homogenate was centrifuged at 1500*g* for 15 min, and the resulting post-nuclear supernatant (PNS) was collected. The PNS from each sample was filtered using a 100-μm cell strainer (Corning) and loaded at the top of a discontinuous step gradient. Each gradient was assembled in an ultra-clear centrifuge tube (14 × 95 mm, Beckman Coulter) in the following sequence from bottom to top: 35% Histodenz (2.6 ml) → 17% Histodenz (2.6 ml) → 6% Percoll (3.9 ml) → PNS (4 ml). The Histodenz and Percoll solutions were made using IB. Gradients were centrifuged using a SW40 Ti rotor/swinging buckets (Beckman Coulter) at 70,000*g* for 45 min (slow acceleration/slow deceleration). The light mitochondrial (LM) fraction (~1.4 ml) at the 17% Histodenz/6% Percoll interface was collected, mixed with 1.1 ml of 80% Histodenz, and loaded at the bottom of a discontinuous step gradient that was assembled in the following sequence from bottom to top: LM fraction (2.5 ml) → 17% Histodenz (2.6 ml) → 5% Histodenz (2.6 ml) → IB (5 ml). Gradients were centrifuged at 70,000*g* for 45 min. The enriched lysosome fraction was collected at the 17% Histodenz/5% Histodenz interface, diluted in IB, and pelleted for 30 min at 100,000*g*. The lysosomal pellet was resuspended in lysis buffer [50 mM tris

(pH 7.5), 1 mM EDTA, 1 mM EGTA, 0.27 M sucrose, 150 mM NaCl, 0.5% NP-40, and protease and phosphatase inhibitors (Roche)], sonicated, and clarified by centrifugation to yield protein lysate.

Proteomics of lysosomal fractions was performed essentially as described previously for mitochondria (*33*). Lysosomal protein lysates (25 μg per replicate) were reduced with 10 mM TCEP (Sigma) for 30 min at room temperature and alkylated with 15 mM chloroacetamide (Sigma) for 30 min at room temperature, and proteins were precipitated using chloroform/methanol. Protein pellets were resuspended in 200 mM EPPS (pH 8.5) and digested with Lys-C (Wako) for 2 hours at 37°C. Trypsin (Promega) was then added to each sample and incubated for an additional 6 hours at 37°C. Lys-C and trypsin were used at a protease:substrate ratio of 1:100 (w/w). Protease reaction was stopped by addition of 5% FA for 30 min. Peptides were dried via vacuum centrifugation and purified by C18 StageTip. Peptides were resuspended in 200 mM EPPS (pH 8.5), quantified using Micro BCA (Thermo Fisher Scientific), and labeled with 11-plex TMT reagents (Thermo Fisher Scientific) for 1 hour at room temperature. Labeling was quenched by addition of 5% hydroxylamine to each reaction and incubation for 15 min. Five percent of the labeled peptides were combined in a ratio check for normalization. Equal amounts of labeled peptides were combined, vacuum dried, and subjected to high-pH reversed-phase fractionation (Thermo Fisher Scientific). The fractions were vacuum dried and purified by C18 StageTip. Peptides were resuspended in 5% ACN/5% FA and analyzed on an Orbitrap Fusion (Thermo Fisher Scientific). Peptides were identified and quantified by a SEQUEST-based in-house tool as described (*26*).

LysoTracker Red staining

The indicated cells were stained with 50 nM LysoTracker Red (Thermo Fisher Scientific, L7528) in DMEM for 30 min at 37°C and washed with PBS three times. Cells were then resuspended in fluorescence-activated cell sorting (FACS) buffer [1% FBS, 1 mM EDTA, and 25 mM Hepes (pH 7) in PBS] containing 4′,6-diamidino-2-phenylindole (DAPI) (10 μM/ml) (Thermo Fisher Scientific) before analysis by flow cytometry (FACSymphony, BD Biosciences).

Statistical analysis

To generate bar graphs, mean and SEM were obtained from values of the indicated sample. To determine statistical significance in Fig. 2I and fig. S3B, *P* value was obtained from one-way analysis of variance (ANOVA) with Greenhouse/Dunnett's multiple comparison correction. These analyses were all performed by using the GraphPad Prism 7 software.

To generate volcano plot in Fig. 2H, individual values were subjected to Welch's *t* test with 1% FDR correction using Perseus (version 1.6.1.3). For Figs. 4 (A and B) and 6C and fig. S2 (A and B), *P* value was determined by using two-tailed *t* test with equal variance in Excel (Microsoft).

SUPPLEMENTARY MATERIALS

Supplementary material for this article is available at http://advances.sciencemag.org/cgi/content/full/4/11/eaav0443/DC1

Fig. S1. Phosphorylation of RAB7A by TBK1.

Fig. S2. Analysis of RAB7A^{S72A} and RAB7A^{S72E} mutants.

Fig. S3. Analysis of PARKIN-dependent mitophagy in RAB7A and FLCN mutant cells.

Data File S1. Phosphoproteomic data for TBK1^{WT} and TBK1$^{-/-}$ cells in response to mitochondrial depolarization (corresponds to experiment in Fig. 1).

Data File S2. Total proteome quantification for cell extracts used in the phosphoproteomic data in Fig. 1 and data file S1.

Data File S3. Phosphoproteome data for PARKIN^{WT} and PARKIN^{S65A} cells, as well as PINK1$^{-/-}$ cells in the presence and absence of depolarization (corresponds to experiment in Fig. 2).

Data File S4. Protein interaction proteomic data for FLAG-HA-RAB7A^{WT}, S72A, and S72E with and without mitochondrial depolarization.

Data File S5. Proteomic data for lysosomes purified from RAB7A^{WT} or RAB7A^{S72A} cells in response to depolarization (corresponds to experiment in Fig. 6).

REFERENCES AND NOTES

1. S. Pickles, P. Vigié, R. J. Youle, Mitophagy and quality control mechanisms in mitochondrial maintenance. *Curr. Biol.* **28**, R170–R185 (2018).
2. J. W. Harper, A. Ordureau, J.-M. Heo, Building and decoding ubiquitin chains for mitophagy. *Nat. Rev. Mol. Cell. Biol.* **19**, 93–108 (2018).
3. S. Sekine, R. J. Youle, PINK1 import regulation; a fine system to convey mitochondrial stress to the cytosol. *BMC Biol.* **16**, 2 (2018).
4. K. Yamano, N. Matsuda, K. Tanaka, The ubiquitin signal and autophagy: An orchestrated dance leading to mitochondrial degradation. *EMBO Rep.* **17**, 300–316 (2016).
5. Y. C. Wong, E. L. F. Holzbaur, Optineurin is an autophagy receptor for damaged mitochondria in parkin-mediated mitophagy that is disrupted by an ALS-linked mutation. *Proc. Natl. Acad. Sci. U.S.A.* **111**, E4439–4448 (2014).
6. M. Lazarou, D. A. Sliter, L. A. Kane, S. A. Sarraf, C. Wang, J. L. Burman, D. P. Sideris, A. I. Fogel, R. J. Youle, The ubiquitin kinase PINK1 recruits autophagy receptors to induce mitophagy. *Nature* **524**, 309–314 (2015).
7. J.-M. Heo, A. Ordureau, J. A. Paulo, J. Rinehart, J. W. Harper, The PINK1-PARKIN mitochondrial ubiquitylation pathway drives a program of OPTN/NDP52 recruitment and TBK1 activation to promote mitophagy. *Mol. Cell* **60**, 7–20 (2015).
8. A. S. Moore, E. L. Holzbaur, Dynamic recruitment and activation of ALS-associated TBK1 with its target optineurin are required for efficient mitophagy. *Proc. Natl. Acad. Sci. U.S.A.* **113**, E3349–3358 (2016).
9. B. Richter, D. A. Sliter, L. Herhaus, A. Stolz, C. Wang, P. Beli, G. Zaffagnini, P. Wild, S. Martens, S. A. Wagner, R. J. Youle, I. Dikic, Phosphorylation of OPTN by TBK1 enhances its binding to Ub chains and promotes selective autophagy of damaged mitochondria. *Proc. Natl. Acad. Sci. U.S.A.* **113**, 4039–4044 (2016).
10. A. Stolz, A. Ernst, I. Dikic, Cargo recognition and trafficking in selective autophagy. *Nat. Cell Biol.* **16**, 495–501 (2014).
11. P. Grumati, I. Dikic, Ubiquitin signaling and autophagy. *J. Biol. Chem.* **293**, 5404–5413 (2018).
12. P. Wild, H. Farhan, D. G. McEwan, S. Wagner, V. V. Rogov, N. R. Brady, B. Richter, J. Korac, O. Waidmann, C. Choudhary, V. Dötsch, D. Bumann, I. Dikic, Phosphorylation of the autophagy receptor optineurin restricts *Salmonella* growth. *Science* **333**, 228–233 (2011).
13. G. Matsumoto, T. Shimogori, N. Hattori, N. Nukina, TBK1 controls autophagosomal engulfment of polyubiquitinated mitochondria through p62/SQSTM1 phosphorylation. *Hum. Mol. Genet.* **24**, 4429–4442 (2015).
14. C. E. Gleason, A. Ordureau, R. Gourlay, J. S. Arthur, P. Cohen, Polyubiquitin binding to optineurin is required for optimal activation of TANK-binding kinase 1 and production of interferon β. *J. Biol. Chem.* **286**, 35663–35674 (2011).
15. T. L. M. Thurston, K. B. Boyle, M. Allen, B. J. Ravenhill, M. Karpiyevich, S. Bloor, A. Kaul, J. Noad, A. Foeglein, S. A. Matthews, D. Komander, M. Bycroft, F. Randow, Recruitment of TBK1 to cytosol-invading *Salmonella* induces WIPI2-dependent antibacterial autophagy. *EMBO J.* **35**, 1779–1792 (2016).
16. K. Yamano, A. I. Fogel, C. Wang, A. M. van der Bliek, R. J. Youle, Mitochondrial Rab GAPs govern autophagosome biogenesis during mitophagy. *eLife* **3**, e01612 (2014).
17. K. Yamano, C. Wang, S. A. Sarraf, C. Munch, R. Kikuchi, N. N. Noda, Y. Hizukuri, M. T. Kanemaki, W. Harper, K. Tanaka, N. Matsuda, R. J. Youle, Endosomal Rab cycles regulate Parkin-mediated mitophagy. *eLife* **7**, e31326 (2018).
18. A. Jimenez-Orgaz, A. Kvainickas, H. Nägele, J. Denner, S. Eimer, J. Dengjel, F. Steinberg, Control of RAB7 activity and localization through the retromer-TBC1D5 complex enables RAB7-dependent mitophagy. *EMBO J.* **37**, 235–254 (2018).
19. K. Hegedus, S. Takáts, A. Boda, A. Jipa, K. Varga, A. L. Kovács, G. Juhász, The Ccz1-Mon1-Rab7 module and Rab5 control distinct steps of autophagy. *Mol. Biol. Cell* **27**, 3132–3142 (2016).
20. C. A. Lamb, T. Yoshimori, S. A. Tooze, The autophagosome: Origins unknown, biogenesis complex. *Nat. Rev. Mol. Cell Biol.* **14**, 759–774 (2013).
21. M. Steger, F. Tonelli, G. Ito, P. Davies, M. Trost, M. Vetter, S. Wachter, E. Lorentzen, G. Duddy, S. Wilson, M. A. Baptista, B. K. Fiske, M. J. Fell, J. A. Morrow, A. D. Reith, D. R. Alessi, M. Mann, Phosphoproteomics reveals that Parkinson's disease kinase LRRK2 regulates a subset of Rab GTPases. *eLife* **5**, e12813 (2016).
22. E. Purlyte, H. S. Dhekne, A. R. Sarhan, R. Gomez, P. Lis, M. Wightman, T. N. Martinez, F. Tonelli, S. R. Pfeffer, D. R. Alessi, Rab29 activation of the Parkinson's disease-associated LRRK2 kinase. *EMBO J.* **37**, 1–18 (2018).
23. R. K. Nookala, L. Langemeyer, A. Pacitto, B. Ochoa-Montaño, J. C. Donaldson, B. K. Blaszczyk, D. Y. Chirgadze, F. A. Barr, J. F. Bazan, T. L. Blundell, Crystal structure of

folliculin reveals a hidDENN function in genetically inherited renal cancer. *Open Biol.* **2**, 120071 (2012).
24. Z. Y. Tsun, L. Bar-Peled, L. Chantranupong, R. Zoncu, T. Wang, C. Kim, E. Spooner, D. M. Sabatini, The folliculin tumor suppressor is a GAP for the RagC/D GTPases that signal amino acid levels to mTORC1. *Mol. Cell* **52**, 495–505 (2013).
25. K. Shen, A. Choe, D. M. Sabatini, Intersubunit crosstalk in the Rag GTPase heterodimer enables mTORC1 to respond rapidly to amino acid availability. *Mol. Cell* **68**, 552–565.e8 (2017).
26. G. C. McAlister, D. P. Nusinow, M. P. Jedrychowski, M. Wühr, E. L. Huttlin, B. K. Erickson, R. Rad, W. Haas, S. P. Gygi, MultiNotch MS3 enables accurate, sensitive, and multiplexed detection of differential expression across cancer cell line proteomes. *Anal. Chem.* **86**, 7150–7158 (2014).
27. A. Ordureau, S. A. Sarraf, D. M. Duda, J. M. Heo, M. P. Jedrychowski, V. O. Sviderskiy, J. L. Olszewski, J. T. Koerber, T. Xie, S. A. Beausoleil, J. A. Wells, S. P. Gygi, B. A. Schulman, J. W. Harper, Quantitative proteomics reveal a feedforward mechanism for mitochondrial PARKIN translocation and ubiquitin chain synthesis. *Mol. Cell* **56**, 360–375 (2014).
28. S. R. Pfeffer, Structural clues to Rab GTPase functional diversity. *J. Biol. Chem.* **280**, 15485–15488 (2005).
29. A. Wandinger-Ness, M. Zerial, Rab proteins and the compartmentalization of the endosomal system. *Cold Spring Harb. Perspect. Biol.* **6**, a022616 (2014).
30. G. Weintz, J. V. Olsen, K. Frühauf, M. Niedzielska, I. Amit, J. Jantsch, J. Mages, C. Frech, L. Dölken, M. M. Mann, R. Lang, The phosphoproteome of toll-like receptor-activated macrophages. *Mol. Syst. Biol.* **6**, 371 (2010).
31. M. Trost, L. English, S. Lemieux, M. Courcelles, M. Desjardins, P. Thibault, The phagosomal proteome in interferon-gamma-activated macrophages. *Immunity* **30**, 143–154 (2009).
32. T. Toyofuku, K. Morimoto, S. Sasawatari, A. Kumanogoh, Leucine-rich repeat kinase 1 regulates autophagy through turning on TBC1D2-dependent Rab7 inactivation. *Mol. Cell. Biol.* **35**, 3044–3058 (2015).
33. C. M. Rose, M. Isasa, A. Ordureau, M. A. Prado, S. A. Beausoleil, M. P. Jedrychowski, D. J. Finley, J. W. Harper, S. P. Gygi, Highly multiplexed quantitative mass spectrometry analysis of ubiquitylomes. *Cell Syst.* **3**, 395–403.e4 (2016).
34. Y.-C. Lai, C. Kondapalli, R. Lehneck, J. B. Procter, B. D. Dill, H. I. Woodroof, R. Gourlay, M. Peggie, T. J. Macartney, O. Corti, J.-C. Corvol, D. G. Campbell, A. Itzen, M. Trost, M. M. K. Muqit, Phosphoproteomic screening identifies Rab GTPases as novel downstream targets of PINK1. *EMBO J.* **34**, 2840–2861 (2015).
35. H. R. Aerni, M. A. Shifman, S. Rogulina, P. O'Donoghue, J. Rinehart, Revealing the amino acid composition of proteins within an expanded genetic code. *Nucleic Acids Res.* **43**, e8 (2015).
36. A. L. Marat, H. Dokainish, P. S. McPherson, DENN domain proteins: Regulators of Rab GTPases. *J. Biol. Chem.* **286**, 13791–13800 (2011).
37. A. Ordureau, J. A. Paulo, W. Zhang, T. Ahfeldt, J. Zhang, E. F. Cohn, Z. Hou, J.-M. Heo, L. L. Rubin, S. S. Sidhu, S. P. Gygi, J. W. Harper, Dynamics of PARKIN-dependent mitochondrial ubiquitylation in induced neurons and model systems revealed by digital snapshot proteomics. *Mol. Cell* **70**, 211–227 (2018).
38. A. Ordureau, J.-M. Heo, D. M. Duda, J. A. Paulo, J. L. Olszewski, D. Yanishevski, J. Rinehart, B. A. Schulman, J. W. Harper, Defining roles of PARKIN and ubiquitin phosphorylation by PINK1 in mitochondrial quality control using a ubiquitin replacement strategy. *Proc. Natl. Acad. Sci. U.S.A.* **112**, 6637–6642 (2015).
39. A. M. Pickrell, R. J. Youle, The roles of PINK1, parkin, and mitochondrial fidelity in Parkinson's disease. *Neuron* **85**, 257–273 (2015).
40. J. H. Weishaupt, T. Hyman, I. Dikic, Common molecular pathways in amyotrophic lateral sclerosis and frontotemporal dementia. *Trends Mol. Med.* **22**, 769–783 (2016).
41. S. R. Shinde S. Maddika, PTEN modulates EGFR late endocytic trafficking and degradation by dephosphorylating Rab7. *Nat. Commun.* **7**, 10689 (2016).
42. L. A. Laviolette, J. Mermoud, I. A. Calvo, N. Olson, M. Boukhali, O. K. Steinlein, E. Roider, E. C. Sattler, D. Huang, B. T. Teh, M. Motamedi, W. Haas, O. Iliopoulos, Negative regulation of EGFR signalling by the human folliculin tumour suppressor protein. *Nat. Commun.* **8**, 15866 (2017).
43. X. Wu, M. J. Bradley, Y. Cai, D. Kümmel, E. M. De La Cruz, F. A. Barr, K. M. Reinisch, Insights regarding guanine nucleotide exchange from the structure of a DENN-domain protein complexed with its Rab GTPase substrate. *Proc. Natl. Acad. Sci. U.S.A.* **108**, 18672–18677 (2011).
44. J. Meng, S. M. Ferguson, GATOR1-dependent recruitment of FLCN-FNIP to lysosomes coordinates Rag GTPase heterodimer nucleotide status in response to amino acids. *J. Cell Biol.* **217**, 2765–2776 (2018).
45. M. Baba, S.-B. Hong, N. Sharma, M. B. Warren, M. L. Nickerson, A. Iwamatsu, D. Esposito, W. K. Gillette, R. F. Hopkins III, J. L. Hartley, M. Furihata, S. Oishi, W. Zhen, T. R. Burke Jr., W. M. Linehan, L. S. Schmidt, B. Zbar, Folliculin encoded by the *BHD* gene interacts with a binding protein, FNIP1, and AMPK, and is involved in AMPK and mTOR signaling. *Proc. Natl. Acad. Sci. U.S.A.* **103**, 15552–15557 (2006).
46. C. Behrends, M. E. Sowa, S. P. Gygi, J. W. Harper, Network organization of the human autophagy system. *Nature* **466**, 68–76 (2010).
47. G. P. Starling, Y. Y. Yip, A. Sanger, P. E. Morton, E. R. Eden, M. P. Dodding, Folliculin directs the formation of a Rab34–RILP complex to control the nutrient-dependent dynamic distribution of lysosomes. *EMBO Rep.* **17**, 823–841 (2016).
48. J. A. Paulo, S. P. Gygi, Isobaric tag-based protein profiling of a nicotine-treated alpha7 nicotinic receptor-null human haploid cell line. *Proteomics* **18**, e1700475 (2018).
49. E. L. Huttlin, M. P. Jedrychowski, J. E. Elias, T. Goswami, R. Rad, S. A. Beausoleil, J. Villén, W. Haas, M. E. Sowa, S. P. Gygi, A tissue-specific atlas of mouse protein phosphorylation and expression. *Cell* **143**, 1174–1189 (2010).
50. S. Tyanova, T. Temu, P. Sinitcyn, A. Carlson, M. Y. Hein, T. Geiger, M. Mann, J. Cox, The Perseus computational platform for comprehensive analysis of (prote)omics data. *Nat. Methods* **13**, 731–740 (2016).
51. C. Aguado, E. Pérez-Jiménez, M. Lahuerta, E. Knecht, Isolation of lysosomes from mammalian tissues and cultured cells. *Methods Mol. Biol.* **1449**, 299–311 (2016).

Acknowledgments
Funding: This work was supported by the NIH (R37 NS083524 and RO1 GM095567 to J.W.H., CA103866 and AI47389 to D.M.S., and K01DK098285 to J.A.P.), the Michael J. Fox Foundation (grant no. 15866 to J.W.H.), an Edward R. and Anne G. Lefler Center Postdoctoral Fellowship (to A.O.), a Sara Elizabeth O'Brien Trust Postdoctoral Fellowship (to J.-M.H.), the Harvard Medical School Cell Biology Initiative for Molecular Trafficking and Neurodegeneration, and a gift from Ned Goodnow (to J.W.H.). D.M.S. is an investigator of the HHMI. **Author contributions:** J.-M.H. and J.W.H. conceived the study. J.-M.H. created cell lines and performed proteomics, biochemical assays, and cell biological analysis. A.O. performed quantitative proteomic experiments. S.S. performed proteomic analysis of lysosomes. J.A.P. performed MS. K.S. performed GAP assays in interaction studies under the direction of D.M.S. The paper was written by J.W.H. and J.-M.H. with input and editing from all authors. **Competing interests:** J.W.H. is a founder and advisory board member of Rheostat Therapeutics and is an advisory board member of X-Chem Inc. The authors declare no other competing interests. **Data and materials availability:** All data needed to evaluate the conclusions in the paper are present in the paper and/or the Supplementary Materials. Additional data related to this paper may be requested from the authors.

Submitted 12 August 2018
Accepted 19 October 2018
Published 21 November 2018
10.1126/sciadv.aav0443

Citation: J.-M. Heo, A. Ordureau, S. Swarup, J. A. Paulo, K. Shen, D. M. Sabatini, J. W. Harper, RAB7A phosphorylation by TBK1 promotes mitophagy via the PINK-PARKIN pathway. *Sci. Adv.* **4**, eaav0443 (2018).